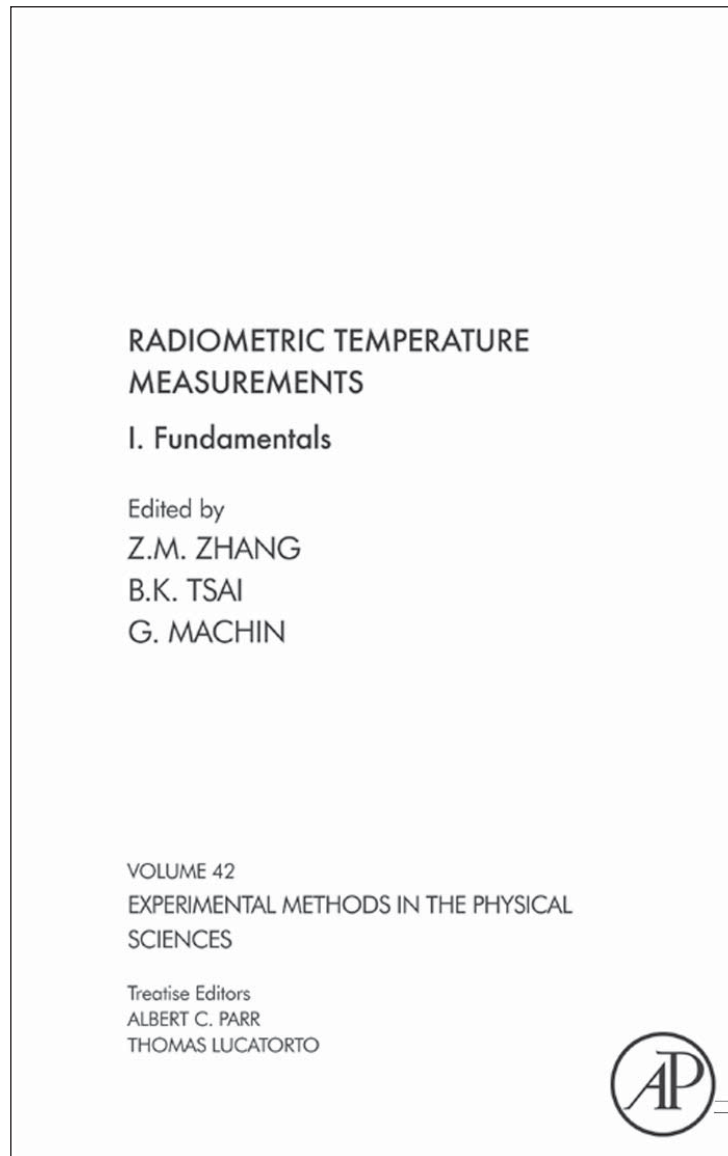


**Provided for non-commercial research and educational use only.  
Not for reproduction, distribution or commercial use.**

This chapter was originally published in the book *Experimental Methods in the Physical Sciences*, published by Elsevier, and the attached copy is provided by Elsevier for the author's benefit and for the benefit of the author's institution, for non-commercial research and educational use including without limitation use in instruction at your institution, sending it to specific colleagues who know you, and providing a copy to your institution's administrator.



All other uses, reproduction and distribution, including without limitation commercial reprints, selling or licensing copies or access, or posting on open internet sites, your personal or institution's website or repository, are prohibited. For exceptions, permission may be sought for such use through Elsevier's permissions site at:

<http://www.elsevier.com/locate/permissionusematerial>

From Alexander V. Prokhorov, Leonard M. Hanssen and Sergey N. Mekhontsev, Calculation of the Radiation Characteristics of Blackbody Radiation Sources. In: Zhuomin M. Zhang, Benjamin Tsai and Graham Machin editors: *Experimental Methods in the Physical Sciences*, Vol 42, Radiometric Temperature Measurements and Applications, Zhuomin M. Zhang, Benjamin Tsai and Graham Machin. The Netherlands: Elsevier, 2010, pp. 181–240.

ISBN: 978-0-12-374021-2

© Copyright 2010 Elsevier Inc.

Academic Press

# CALCULATION OF THE RADIATION CHARACTERISTICS OF BLACKBODY RADIATION SOURCES<sup>☆</sup>

Alexander V. Prokhorov, Leonard M. Hanssen *and*  
Sergey N. Mekhontsev

## Contents

1. Introduction	181
2. Definitions of Principal Quantities	182
3. Deterministic Methods	187
3.1. Approximate expressions for isothermal diffuse cavities	187
3.2. Method of integral equations for diffuse cavities	189
3.3. Integrated effective emissivity of diffuse cavities	199
3.4. Series technique for multiple reflections in cavities	201
3.5. Cavities with diffusely emitting and specularly reflecting walls	204
3.6. Specular–diffuse cavities	205
3.7. Method of successive reflections	205
4. Monte Carlo Method	208
4.1. Stochastic approach to radiative heat transfer	208
4.2. Ray tracing	210
4.3. Stochastic models for optical properties	211
4.4. Monte Carlo modeling of specular–diffuse blackbodies	212
4.5. Modeling of direction-dependent optical characteristics	227
5. Numerical Comparison of Results Obtained by Various Methods	231
6. Conclusions	233
Acknowledgement	234
References	234

<sup>☆</sup>Certain commercial software is identified in this paper in order to specify the computational procedure adequately. Such identification is not intended to imply recommendation or endorsement by the National Institute of Standards and Technology, nor is it intended to imply that the software identified is necessarily the best available for the purpose.

National Institute of Standards and Technology, 100 Bureau Drive, Gaithersburg, MD 20899-8442, USA

*Experimental Methods in the Physical Sciences*, Volume 42  
ISSN 1079-4042, DOI 10.1016/S1079-4042(09)04205-2

© 2010 Elsevier Inc.  
All rights reserved.

## 1. INTRODUCTION

A source of optical radiation whose radiation characteristics can be calculated on the basis of fundamental physical laws makes possible the calibration of radiation thermometers in absolute units of temperature. Theoretically, a perfect blackbody is the most suitable object for this purpose. At the same time, a perfect blackbody is an “ideal” object, that is, not more than a physical abstraction that does not exist in the real world. It is well known that the perfect blackbody conditions are realized inside a closed isothermal cavity with opaque walls (see, for instance, Refs. [1–4]).

However, the blackbody radiation of a closed cavity is inaccessible and unobservable. Thus, instead of using a completely enclosed cavity, one can approach the ideal by leaving only a small opening in the cavity. The radiation escaping the cavity through the opening will then very closely mimic blackbody radiation. From this point forward, we shall use the term *blackbody* for a real radiator whose radiation properties approach those of a perfect blackbody. This term is equivalent to the following terms found frequently within the technical literature: *blackbody radiation source*, *blackbody reference source*, *blackbody calibration source*, *blackbody simulator*, *artificial blackbody*, *imperfect blackbody*, *laboratory blackbody*, etc.

In order to employ a blackbody as a standard reference source for radiation thermometry, it is necessary to know how large the differences are between the radiation characteristics of the blackbody – for a given geometry and cavity wall material – and those of a perfect blackbody. Radiometry, radiation thermometry, optical remote sensing, and other areas of modern science and technology require determination of the effective emissivity of blackbody calibration sources with a relative uncertainty of 0.01% or less. Similar requirements of accuracy are necessary for radiance temperature and other quantities employed in the design, characterization, and calibration of blackbody radiators.

Due to the difficulty of performing accurate measurements, computational methods have, until recently, remained the primary mode of investigation of blackbody radiation characteristics, for those deviating only slightly from a perfect blackbody.

This chapter is devoted to the computational characterization of radiation emitted by blackbodies. We shall emphasize work of the last two decades (1990s and 2000s), while still including earlier milestone work. The interested reader may refer to an excellent survey [5] for information regarding work reported prior to 1982. Useful information can also be found in additional overviews in Refs. [6–8].

Section 2 describes the terminology we use and provides definitions of principal quantities used in this chapter. Conventional, deterministic methods for calculation of the radiation characteristics of isothermal and nonisothermal

cavities are considered in Section 3. The applications of these methods are primarily determined by the model of radiation characteristics (diffuse, specular, etc.) adopted for the cavity walls. Section 4 describes the application of the stochastic (Monte Carlo) ray-tracing method to computer modeling of blackbody radiators. This computational method has become prevalent in the last decades of the 20th century due to its great generality, flexibility, and a number of other advantages. In Section 5, a comparison of some results obtained by various methods is described.

## 2. DEFINITIONS OF PRINCIPAL QUANTITIES

The quantitative measure for the difference in the radiation characteristics between an artificial blackbody and a perfect one is the *effective emissivity* (sometimes, the terms *apparent emissivity* or *cavity's emissivity* are used; we shall consider all these terms as interchangeable). The qualifier *effective* is used due to the effect produced by multiple reflections. Unlike in the case of a flat sample, the outgoing radiation of an element of the cavity wall consists not only of its own thermal radiation, but also of radiation falling from other surface elements and reflected by the element under consideration. Generally speaking, the effective emissivity is the ratio of a radiometric quantity (usually, radiance or spectral radiance) that characterizes the blackbody at a certain temperature to the same quantity of a perfect blackbody having the same temperature. Real-world cavities are always nonisothermal. Temperature nonuniformity might significantly change the cavity radiation characteristics. The effective emissivity of a nonisothermal cavity is a function of a temperature assigned to the perfect blackbody in the effective emissivity definition (often referred to as the *reference temperature*) and might be less than or greater than unity, depending on the assigned reference temperature.

Let us consider an isothermal cavity with a small opening. The radiation escaping the cavity through this opening differs little from the radiation of a perfect blackbody. Due to the geometrical invariance of the spectral radiance along rays, the spectral radiance of the opening is equal to that of the cavity internal surface projected by the rays passed through the opening in opposite directions. In its turn, the outgoing radiation flux from the cavity wall toward the opening consists of two parts: the flux of the surface element's own thermal emission and the flux reflected by this element. The first part depends only on the emissivity and temperature of the cavity wall and does not depend upon the presence of the rest of the cavity. The reflected flux depends on the surface element reflectance and on the radiation flux falling onto this element from the rest of the cavity. The opening affects the reflected flux, because the radiant flux that should arrive from the wall of the closed cavity is absent if the opening is present.

Moreover, in the case of a cavity with the opening, the radiation flux propagated from the opening to the rest of the cavity is also absent. Accordingly, the irradiation of a target area from the rest of the cavity is somewhat lower than that in the case of a closed cavity. The net result is that the radiation flux exiting from the isothermal cavity is greater than that of a flat sample having the same temperature and made of the same material as the cavity, but less than the radiation flux of a perfect blackbody at the same temperature. The increase of the radiation flux of a blackbody in comparison with a flat sample is known as the *cavity effect*.

Now, we shall define the most important quantities that characterize blackbody radiation sources. Unless otherwise specified, we shall assume that the environment is nonrefracting, nonabsorbing, nonscattering, and nonemitting (i.e., vacuum at 0 K), or that these effects are negligible. We will also assume that the optical properties of the cavity wall do not depend on temperature.

The effective emissivity of a blackbody may be defined in a variety of ways depending on the variables one considers. First, let us consider radiation emitted from a point on the blackbody wall at a particular wavelength,  $\lambda$ , with coordinates specified by the vector  $\boldsymbol{\xi}$ , and the direction in which the radiation is emitted is given by the vector  $\boldsymbol{\omega}$ . Under these conditions, the effective emissivity,  $\varepsilon_e$ , is defined by the following equation:

$$\varepsilon_e(\lambda, \boldsymbol{\xi}, \boldsymbol{\omega}, T_0) = \frac{L_\lambda(\lambda, \boldsymbol{\xi}, \boldsymbol{\omega})}{L_{\lambda, \text{bb}}(\lambda, T_0)} \quad (1)$$

where  $L_\lambda$  and  $L_{\lambda, \text{bb}}$  are the spectral radiances (in  $\text{W}/(\text{m}^2 \text{sr})$ ) of the blackbody being considered and a perfect blackbody at a reference temperature  $T_0$ .

In Ref. [5], the definition of spectral directional effective emissivity is formulated using the spectral exitance  $M_\lambda$  for which, however, the dependence on direction is indicated. This represents a confusion of terminology. The spectral exitance can be employed in definitions only for blackbodies with Lambertian (diffusely emitting and reflecting) internal walls; the rigorous definition for a blackbody with an arbitrary angular distribution of emitted and reflected radiation requires the use of radiance.

The denominator in Equation (1) is defined according to Planck's law:

$$L_{\lambda, \text{bb}}(\lambda, T_0) = \frac{c_1}{\pi \lambda^5 [\exp(c_2/(\lambda T_0)) - 1]} \quad (2)$$

where  $c_1$  and  $c_2$  are the first and second radiation constants, respectively [9].

This quantity of effective emissivity, which defines local, directional, and spectral properties, is the primary radiation characteristic of a blackbody cavity. Other kinds of effective emissivities can be obtained by averaging over the spatial, angular, and spectral domains. For example, integration over a finite spectral range  $[\lambda_1, \lambda_2]$  results in the following equation for the

bandlimited effective emissivity:

$$\varepsilon_e(\lambda, \lambda_1, \lambda_2, \xi, \omega, T_0) = \frac{\int_{\lambda_1}^{\lambda_2} L_\lambda(\lambda, \xi, \omega) d\lambda}{\int_{\lambda_1}^{\lambda_2} L_{\lambda,bb}(\lambda, \xi, \omega, T_0) d\lambda} \quad (3)$$

Similarly, integration over the entire spectrum of radiation reduces the equation to a ratio of radiances. Application of the Stefan–Boltzmann law further simplifies the equation to:

$$\varepsilon_e(\xi, \omega, T_0) = \frac{\pi L(\xi, \omega)}{\sigma T_0^4} \quad (4)$$

where  $L$  is the radiance of the cavity wall and  $\sigma$  is the Stefan–Boltzmann constant [9].

One can also integrate with respect to the solid angle, over a hemisphere. This transforms the term for spectral radiance,  $L_\lambda$ , to spectral radiant exitance,  $M_\lambda$ . Thus, the spectral hemispherical effective emissivity at a particular wavelength,  $\lambda$ , is then defined as

$$\varepsilon_{e,h}(\lambda, \xi, T_0) = \frac{M_\lambda(\lambda, \xi)}{M_{\lambda,bb}(\lambda, T_0)} = \frac{M_\lambda(\lambda, \xi)}{\pi L_{\lambda,bb}(\lambda, T_0)} \quad (5)$$

Further integration over a bandwidth of radiation or the complete spectrum results in bandlimited and total hemispherical effective emissivities:

$$\varepsilon_{e,h}(\lambda, \xi, T_0) = \frac{\int_{\lambda_1}^{\lambda_2} M_\lambda(\lambda, \xi) d\lambda}{\int_{\lambda_1}^{\lambda_2} M_{\lambda,bb}(\lambda, \xi) d\lambda} = \frac{\int_{\lambda_1}^{\lambda_2} M_\lambda(\lambda, \xi) d\lambda}{\pi \int_{\lambda_1}^{\lambda_2} L_{\lambda,bb}(\lambda, \xi) d\lambda} \quad (6)$$

$$\varepsilon_{e,h}(\xi, T_0) = \frac{M(\xi)}{M_{bb}(T_0)} = \frac{M(\xi)}{\sigma T_0^4} \quad (7)$$

In some situations it is useful to know the *spectral integrated effective emissivity*. This quantity,  $\varepsilon_{e,c}$ , is the ratio of the spectral radiation flux falling onto the detector from a blackbody,  $\Phi_\lambda$ , to the spectral radiation flux,  $\Phi_{\lambda,bb}$ , from a perfectly black surface that replaces the blackbody aperture and has the temperature  $T_0$ :

$$\varepsilon_{e,c}(\lambda, T_0) = \frac{\Phi_\lambda(\lambda)}{\Phi_{\lambda,bb}(\lambda, T_0)} \quad (8)$$

Integration over a bandwidth of radiation or the complete spectrum results in bandlimited and total integrated effective emissivities:

$$\varepsilon_{e,c}(\lambda, \lambda_1, \lambda_2, T_0) = \frac{\int_{\lambda_1}^{\lambda_2} \Phi_\lambda(\lambda) d\lambda}{\int_{\lambda_1}^{\lambda_2} \Phi_{\lambda,bb}(\lambda, T_0) d\lambda} \quad (9)$$

$$\varepsilon_{e,c}(T_0) = \frac{\Phi}{\Phi_{bb}(T_0)} \quad (10)$$

A common calibration method, which does not utilize optical elements, is composed of a blackbody with a circular aperture of radius,  $R_a$ , and a circular detector of radius,  $R_d$ . The aperture and detector are coaxial, lying on two parallel planes separated by a distance,  $H_d$ . In the limiting case where  $R_d = R_a$  and  $H_d \rightarrow \infty$ , we refer to the quantity  $\varepsilon_{e,n}$ , the *normal effective emissivity*. If  $R_d = R_a$  and  $H_d \rightarrow 0$ , then we refer to, the hemispherical effective emissivity,  $\varepsilon_{e,h}$ . The latter characterizes the overall radiative heat loss of a cavity through its aperture.

Depending on the particular viewing conditions that are used for various types of radiation thermometers, pyrometers, radiometers, etc., one can define the appropriate types of effective emissivities by averaging the local directional effective emissivity over a visible part of the cavity internal surface and a suitable solid angle.

All the previous definitions have been developed for a nonradiating background environment. However, real environments have temperatures greater than absolute zero. Therefore, thermal radiation from the surrounding environment will irradiate the aperture of a blackbody cavity and can fall onto the detector after multiple reflections inside the cavity. Because the spectral, spatial, and angular distributions of background radiation are hard to predict, one usually considers the simplest case of isotropic blackbody radiation corresponding to the background temperature,  $T_{bg}$ . Assuming that the detector does not distort the isotropy of the background radiation, the effect of the background radiation on the spectral local directional effective emissivity of a nonisothermal blackbody can be taken into account by the second term in the equation:

$$\begin{aligned} \varepsilon_e(\lambda, \xi, \omega, T_0, T_{bg}) \\ = \varepsilon_e(\lambda, \xi, \omega, T_0) + [1 - \varepsilon_e(\lambda, \xi, \omega)] \frac{\exp(c_2/(\lambda T_0)) - 1}{\exp(c_2/(\lambda T_{bg})) - 1} \end{aligned} \quad (11)$$

Here  $\varepsilon_e(\lambda, \xi, \omega, T_0, T_{bg})$  is the spectral effective emissivity of a nonisothermal blackbody taking into account the background radiation;  $\varepsilon_e(\lambda, \xi, \omega, T_0)$  does not include this correction;  $\varepsilon_e(\lambda, \xi, \omega)$  is the spectral effective emissivity of an isothermal blackbody.

By analogy, the bandlimited and total effective emissivities of a nonisothermal blackbody taking into account the background radiation can be defined by the equations:

$$\begin{aligned} \varepsilon_e(\lambda, \lambda_1, \lambda_2, \xi, \omega, T_0, T_{bg}) \\ = \varepsilon_e(\lambda, \lambda_1, \lambda_2, \xi, \omega, T_0) + [1 - \varepsilon_e(\lambda, \lambda_1, \lambda_2, \xi, \omega)] \frac{\int_{\lambda_1}^{\lambda_2} L_{\lambda,bb}(\lambda, T_{bg}) d\lambda}{\int_{\lambda_1}^{\lambda_2} L_{\lambda,bb}(\lambda, T_0) d\lambda} \end{aligned} \quad (12)$$

and

$$\varepsilon_e(\xi, \omega, T_0, T_{bg}) = \varepsilon_e(\xi, \omega, T_0) + [1 - \varepsilon_e(\xi, \omega, T_0)] \left( \frac{T_{bg}}{T_0} \right)^4 \quad (13)$$

Another important quantity is the *radiance temperature*,  $T_S$ , that is defined as the temperature of a perfect blackbody, for which the spectral radiance at the specified wavelength  $\lambda$  has the same value as for the thermal radiator under consideration. For an imperfect blackbody having the spectral effective emissivity  $\varepsilon_e$ , the radiance temperature can be computed as

$$T_S(\lambda, \xi, \omega) = c_2 \left\{ \lambda \ln \left[ 1 + \frac{\exp(c_2/(\lambda T_0)) - 1}{\varepsilon_e(\lambda, \xi, \omega, T_0)} \right] \right\}^{-1} \quad (14)$$

Rather than identifying the temperature associated with a particular wavelength, we can also identify the temperature at which the radiance emitted from a perfect blackbody is equal to the radiance emitted from a blackbody radiator. This temperature is referred to as the *radiation temperature*,  $T_R$ :

$$T_R(\xi, \omega) = T_0 \sqrt[4]{\varepsilon_e(\xi, \omega, T_0)} \quad (15)$$

The equations defining the radiance and radiation temperatures for different viewing conditions can be written by analogy to the equivalent types of effective emissivity.

In this section, we have considered only a portion of the characteristics describing the radiation of blackbody radiators that appear in published works. There has been no unified system presented in literature for terminology used in this section that is similar to the nomenclature developed by Nicodemus et al. [10] for material optical properties. Definitions concerned with the viewing conditions using an optical system are completely absent. This can sometimes lead to serious difficulties when comparing the results obtained by independent researchers. At the same time, we have not attempted to establish a comprehensive terminology for the radiation characteristics of blackbodies, but rather to provide useful terms and clarity about their meaning. In the following sections, we shall consider the principal methods used for calculating the radiation characteristics that we have defined above.



### 3. DETERMINISTIC METHODS

#### 3.1. Approximate expressions for isothermal diffuse cavities

The first and simplest approximate analytical expressions were derived for an isothermal cavity whose internal surface emits and reflects optical radiation according to Lambert's law (diffuse cavity approximation).

If Kirchoff's law holds for effective characteristics of a cavity (see Refs. [11,12] for detailed discussions), then to calculate the normal effective emissivity  $\varepsilon_{e,n}$  of a cavity, it is sufficient to compute its normal effective absorptance  $\alpha_{e,n}$  (or normal effective reflectance,  $\rho_{e,n}$ , since  $\alpha_{e,n} + \rho_{e,n} = 1$  for opaque cavity walls). In other words,

$$\varepsilon_{e,n} = \alpha_{e,n} = 1 - \rho_{e,n} \quad (16)$$

for a beam of radiation falling into the cavity perpendicularly to its aperture.

Ribaud [13] considered only the first reflection; assuming that all radiation is absorbed by the cavity after a single reflection, he obtained:

$$\varepsilon_{e,n} = 1 - \rho \frac{\Omega}{\pi} \quad (17)$$

where  $\rho$  is the reflectance of a cavity wall and  $\Omega$  the solid angle subtended by the cavity aperture from the center of the area irradiated by an infinitely thin incident ray.

Gouffé [14] considered a cavity of arbitrary shape, with an aperture area,  $s$ , and a total surface area,  $S$  (aperture included). Gouffé assumed that the reflected radiation is uniformly distributed over the cavity walls from each reflection. Summing the radiation fluxes escaping the cavity following each reflection, and using the expression for an infinite geometric progression, he obtained the following formula for the effective emissivity:

$$\varepsilon_e = \frac{\varepsilon[1 + (1 - \varepsilon)((s/S) - (\Omega/\pi))]}{\varepsilon(1 - (s/S)) + (s/S)} \quad (18)$$

where  $\varepsilon = 1 - \rho$ .

Equation (18) gives the exact value of the effective emissivity for the case of an isothermal diffuse spherical cavity because the assumption that the reflected radiation is uniformly distributed over the cavity walls from each reflection is correct for a spherical cavity. For a sphere,  $s/S = \Omega/\pi$  and Equation (18) can be rewritten as:

$$\varepsilon_e = \frac{\varepsilon}{\varepsilon(1 - (s/S)) + (s/S)} \quad (19)$$

Treuenfels [15] represented the effective emissivity of a diffuse cavity in the form:

$$\varepsilon_e = 1 - \sum_{k=1}^{\infty} f_k \rho^k \quad (20)$$

where  $f_k$  is the fraction of the radiation flux, reflected  $k$  times before emerging from the cavity and

$$\sum_{k=1}^{\infty} f_k = 1 \quad (21)$$

Treuenfels made an assumption that the ratio of successive fractions,  $\beta = f_{k+1}/f_k$ , is constant and always less than 1, from which he derived the following form for the effective emissivity:

$$\varepsilon_e = \frac{\varepsilon}{\varepsilon + f_1(1 - \varepsilon)} \quad (22)$$

Equation (22) is the equivalent of Equation (19), if  $s/S$  is substituted for  $f_1$ . For a variety of simple geometric shapes,  $f_1$  can be evaluated using

$$f_1 = \frac{\int_A F_{\xi s}^2 dA}{\int_A F_{\xi s} dA} \quad (23)$$

where  $A = S - s$  is the cavity radiating surface area and  $F_{\xi s}$  is the *diffuse view factor* [3,4] from a surface element  $dA$  at a position  $\xi$  to the aperture  $s$  that is equal to the ratio of the radiation flux diffusely emitted by  $dA$  into the hemisphere to its fraction falling onto the aperture (other terms used are angle factor [1], configuration factor [2], and form factor [16]). Using analytical integration, Treuenfels obtained expressions for  $f_1$  for several simple geometries such as a spherical cavity, and infinite grooves of cylindrical, triangular, and rectangular profiles.

Despite the improved sophistication of Treuenfels' method as compared to Gouffé's method, it does not provide an assured increase of the accuracy for calculation of the effective emissivity of an arbitrarily shaped cavity. In addition, neither of these methods takes into account the real temperature distribution over cavity's radiating surface.

### 3.2. Method of integral equations for diffuse cavities

The internal walls of diffuse cavities emit and reflect optical radiation according to Lambert's cosine law. Let us consider a diffuse cavity (see Figure 1).

For simplicity, we shall assume the radiative characteristics to be temperature independent and uniform over the entire cavity surface. The element  $dA$  of a cavity surface  $A$  at the point  $\xi$  has the temperature  $T(\xi)$ . The outgoing radiation of the element  $dA$  consists of its own thermal radiation and the radiation falling onto the element  $dA$  from the remainder of a surface  $A$ . The *surface density* (or *radiosity*)  $B$  of the outgoing radiation flux can be expressed as [1]:

$$B(\xi) = \varepsilon\sigma T^4(\xi) + (1 - \varepsilon)E(\xi) \quad (24)$$

where  $E(\xi)$  is the irradiance of the element  $dA$  produced by the rest of the cavity's internal surface.

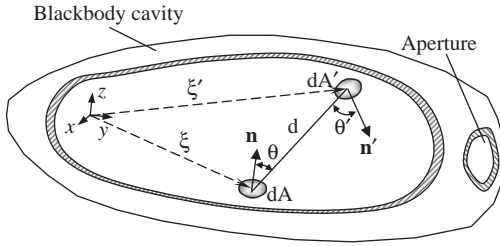


**Figure 1** Drawing for derivation of the equation for effective emissivity.  $\mathbf{n}$  and  $\mathbf{n}'$  are the normals to the surface elements  $dA$  and  $dA'$ , respectively.

It is defined as

$$E(\xi) = \int_A B(\xi') dF_{dA-dA'}(\xi, \xi') \tag{25}$$

where the integration occurs over the entire cavity's radiating surface  $A$  and

$$dF_{dA-dA'} = \frac{\cos\theta \cos\theta'}{\pi d^2} dA' \tag{26}$$

is the differential view factor between elements  $dA$  at  $\xi$  and  $dA'$  at  $\xi'$ (see Figure 1). By substituting Equation (25) into Equation (24), we obtain:

$$B(\xi) = \varepsilon\sigma T^4(\xi) + (1 - \varepsilon) \int_A B(\xi') dF_{dA-dA'}(\xi, \xi') \tag{27}$$

The local hemispherical effective emissivity of a cavity wall is defined as

$$\varepsilon_{e,h}(\xi, T_0) = \frac{B(\xi)}{\sigma T_0^4} \tag{28}$$

For a cavity with perfectly diffuse walls, the local hemispherical effective emissivity is equal to the local directional effective emissivity; therefore we can omit the subscript “ $h$ ” in the left-hand side of Equation (28). After substituting Equation (27) into Equation (28), we obtain:

$$\varepsilon_e(\xi, T_0) = \varepsilon \left[ \frac{T(\xi)}{T_0} \right]^4 + (1 - \varepsilon) \int_A \varepsilon_e(\xi', T_0) K(\xi, \xi') dA' \tag{29}$$

where  $K(\xi, \xi') = dF_{dA-dA'}(\xi, \xi')/dA'$  is the kernel of the linear integral equation, in which the unknown function  $\varepsilon_e(\xi, T_0)$  is placed inside the integral sign. For an isothermal cavity, Equation (29) can be rewritten in the form:

$$\varepsilon_e(\xi) = \varepsilon + (1 - \varepsilon) \int_A \varepsilon_e(\xi') K(\xi, \xi') dA' \tag{30}$$

By introducing the *spectral radiosity*

$$B_\lambda(\lambda, \xi) = \frac{c_1(\lambda)}{\lambda^5 [\exp(c_2/(\lambda T(\xi))) - 1]} + [1 - \varepsilon(\lambda)]E_\lambda(\lambda, \xi) \quad (31)$$

which is the sum of the spectral exitance of thermal radiation, emitted from a diffuse surface element with a spectral emissivity  $\varepsilon(\lambda)$ , and the reflected portion of the incident spectral irradiance  $E_\lambda$ . One can write the analogs of Equations (29) and (30) for the spectral effective emissivity of a nonisothermal and an isothermal cavity:

$$\varepsilon_e(\lambda, \xi, T_0) = \varepsilon(\lambda) \frac{\exp(c_2/(\lambda T_0)) - 1}{\exp(c_2/(\lambda T(\xi))) - 1} + [1 - \varepsilon(\lambda)] \int_A \varepsilon_e(\lambda, \xi', T_0) K(\xi, \xi') dA' \quad (32)$$

$$\varepsilon_e(\lambda, \xi) = \varepsilon(\lambda) + [1 - \varepsilon(\lambda)] \int_A \varepsilon_e(\lambda, \xi') K(\xi, \xi') dA' \quad (33)$$

Equations (32) and (33) must be solved for every value of wavelength  $\lambda$ . Mathematically, the equations presented above all have the form of a Fredholm's integral equation of second kind:

$$\varepsilon_e(\xi) - \rho \int_a^b K(\xi, \xi') \varepsilon_e(\xi') d\xi' = \Lambda(\xi) \quad (34)$$

where  $\rho = 1 - \varepsilon$ ,  $a \leq \xi, \xi' \leq b$ , and

$$\Lambda(\xi) = \begin{cases} \varepsilon \text{ for an isothermal blackbody} \\ \varepsilon(\lambda) \frac{\exp(c_2/(\lambda T_0)) - 1}{\exp(c_2/(\lambda T(\xi))) - 1} \text{ for the spectral effective emissivity} \\ \varepsilon \left[ \frac{T(\xi)}{T_0} \right]^4 \text{ for the total effective emissivity} \end{cases} \quad (35)$$

A variety of methods, analytical and numerical, have been developed (e.g., see Refs. [17–19]) for solving equations of the form of Equation (34). Only two geometrical configurations are known to have exact analytical solutions. The first is a diffuse concave cylindrical groove. Its radiative properties were comprehensively studied in Ref. [20]. The second is a spherical cavity [21]. The sphere has a notable property: the view factor between two surface elements, infinitesimal or finite, does not depend on their positions. Thus,

$$dF_{dA-dA'} = dF_{A-dA'} = \frac{dA'}{4\pi R^2} \quad (36)$$

and

$$F_{dA-A'} = F_{A-A'} = \frac{A'}{4\pi R^2} \quad (37)$$

where  $R$  is the sphere radius.

After substitution of Equation (36) into Equation (27) and simple transformations, for isothermal spherical cavity, we obtain

$$\varepsilon_c = \frac{\varepsilon}{1 - (1/2)(1 - \varepsilon)(1 + \cos\phi)} \quad (38)$$

where  $\phi$  is the opening half-angle. It is easy to show that Equation (38) is equivalent to Equation (19) (Gouffé formula). The closed-form solution for the nonisothermal diffuse spherical cavity can be found in Ref. [22]. In particular, for axisymmetrical distributions of temperature  $T(x)$  and the wall's emissivity  $\varepsilon(\lambda, x)$ , the spectral radiosity can be expressed as

$$B_\lambda(\lambda, x) = \varepsilon(\lambda, x)L_{\lambda,bb}(\lambda, T(x)) + \frac{[1 - \varepsilon(\lambda, x)] \int_0^{x_0} \varepsilon(\lambda, x')L_{\lambda,bb}(\lambda, T(x')) dx'}{2R - \int_0^{x_0} [1 - \varepsilon(\lambda, x')] dx'} \quad (39)$$

All the geometrical parameters are shown in Figure 2. By dividing both sides of Equation (39) by  $L_{\lambda,bb}(\lambda, T_0)$ , we can obtain the expression for the local effective emissivity.

A number of approximate methods for solving Equations (29) and (32) have been developed in precomputer era. However, they are of historical interest only due to the significant difficulty of analytical integration and the unsatisfactory accuracy of the results.

We shall consider three numerical methods that, in principle, allow us to obtain exact solutions, assuming no limitations on computing time,

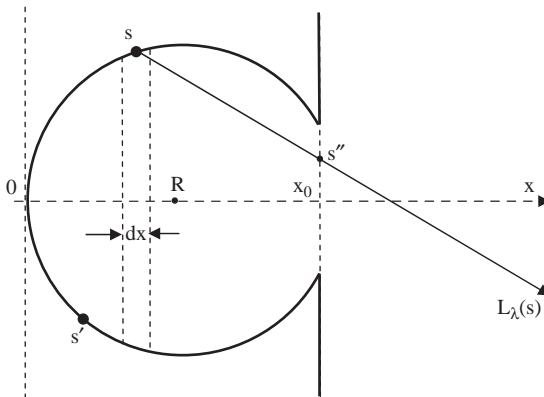


**Figure 2** Geometry of a nonisothermal spherical cavity (from Ref. [22]).

rounding errors, etc. The first method is the *method of iterations* (or the *method of successive approximations*). Let us rewrite Equation (34) in the form

$$\varepsilon_c(\xi) = \rho \int_a^b K(\xi, \xi') \varepsilon_c(\xi') d\xi' + \varphi(\xi) \quad (40)$$

By substitution into the right-hand side of Equation (40) of an arbitrary continuous trial function  $\varepsilon_c^{(0)}(\xi)$  instead of  $\varepsilon_c(\xi)$ , we will obtain

$$\varepsilon_c^{(1)}(\xi) = \rho \int_a^b K(\xi, \xi') \varepsilon_c^{(0)}(\xi') d\xi' + \varphi(\xi) \quad (41)$$

Successive repetition of this process results in

$$\varepsilon_c^{(n)}(\xi) = \rho \int_a^b K(\xi, \xi') \varepsilon_c^{(n-1)}(\xi') d\xi' + \varphi(\xi) \quad (42)$$

where  $\varepsilon_c^{(n)}(\xi)$ ,  $n = 1, 2, \dots$  are successive approximations to the solution of Equation (30).

Note that Equation (42) reduces to Equation (40) in the limit that  $\varepsilon_c^{(n)}(\xi) \rightarrow \varepsilon_c(\xi)$  for  $n \rightarrow \infty$ . Usually, the integration is performed numerically. Assuming that  $\varepsilon_c^{(0)} = 0$  and  $\varepsilon_c^{(1)} = \varepsilon$ , we can transform Equation (43) to the form [23]:

$$\varepsilon_c^{(n)}(\xi) = \varepsilon_c^{(n-1)}(\xi) + \rho \int_a^b K(\xi, \xi') [\varepsilon_c^{(n-1)}(\xi') - \varepsilon_c^{(n-2)}(\xi')] d\xi' \quad (43)$$

Numerical integration is performed with the help of one of the quadrature formulas. Although Equation (43) requires the use of the results of two preceding iterations for each step, convergence of the iteration process itself is improved.

The second method is the *series method*. We assume the solution of Equation (34) to be of the form

$$\varepsilon_c(\xi) = \Lambda(\xi) + \sum_{k=1}^{\infty} \rho^k E_k(\xi) \quad (44)$$

After substitution of Equation (44) into Equation (34) and collecting the coefficients of equal powers of  $\rho$ , we obtain the recurrent system of equations for the functions  $E_k(\xi)$ :

$$\begin{aligned} E_1(\xi) &= \int_a^b K(\xi, \xi') \Lambda(\xi') d\xi' \\ E_2(\xi) &= \int_a^b K(\xi, \xi') E_1(\xi') d\xi' = \int_a^b K_2(\xi, \xi') \Lambda(\xi') d\xi' \\ E_3(\xi) &= \int_a^b K(\xi, \xi') E_2(\xi') d\xi' = \int_a^b K_3(\xi, \xi') \Lambda(\xi') d\xi' \\ &\dots \\ E_k(\xi) &= \int_a^b K(\xi, \xi') E_{k-1}(\xi') d\xi' = \int_a^b K_k(\xi, \xi') \Lambda(\xi') d\xi' \end{aligned} \quad (45)$$

where

$$K_1(\xi, \xi') = K(\xi, \xi'), \quad K_k(\xi, \xi') = \int_a^b K(\xi, \xi'') K_{k-1}(\xi'', \xi') d\xi'', \quad k = 2, 3, \dots \quad (46)$$

are the iterated kernels of the integral equation. Rewriting Equation (44) in terms of Equations (45) and (46) results in the *Neumann series*:

$$\varepsilon_e(\xi) = \Lambda(\xi) + \sum_{k=1}^{\infty} \rho^k \int_a^b K_k(\xi, \xi') \Lambda(\xi') d\xi' \quad (47)$$

Sydnor in Ref. [24] notes that the series representation, in the special case of wavelength-dependent surface emissivity, offers a significant saving in computation time for the evaluation of a large number of monochromatic values  $\varepsilon_e(\lambda, \xi)$ .

The third approach to solving Equation (34) is the *quadrature method*. In this method, the linear integral equation is reduced to the system of linear algebraic equations using one of the quadrature formulas (usually, Simpson's or the trapezoidal rule) for the integral calculations. Generally, the quadrature formula can be written in the form:

$$\int_a^b z(\xi) dx = \sum_{i=1}^n A_i z(\xi_i) + \Delta_n[z] \quad (48)$$

where  $\xi_i$  ( $i = 1, 2, \dots, n$ ) are the nodes of the quadrature on the interval  $[a, b]$ ,  $A_i \geq 0$  are the weighting factors that do not depend upon  $z(\xi)$ ,  $\sum_{i=1}^n A_i = b - a$ , and  $\Delta_n[z]$  is the remainder term.

If the remainder term is negligible, one can rewrite Equation (34) as the system of  $n$  linear algebraic equations with the  $n$  variables  $\varepsilon_i = \varepsilon(\xi_i)$  such that

$$\varepsilon_{e,k} - \rho \sum_{i=1}^n A_i K(\xi_k, \xi_i) \varepsilon_{e,i} = \Lambda_k, \quad k = 1, 2, \dots, n \quad (49)$$

where  $\Lambda_k = \Lambda(\xi_k)$ ,  $K_{ki} = K(\xi_k, \xi_i)$ . Equation (49) can be written in an equivalent form:

$$\sum_{i=1}^n [\delta_{ik} - \rho A_i K_{ki}] \varepsilon_{e,i} = \Lambda_k, \quad k = 1, 2, \dots, n \quad (50)$$

where  $\delta_{ik}$  is the Kronecker delta, defined as

$$\delta_{ik} = \begin{cases} 1, & \text{when } i = k \\ 0, & \text{when } i \neq k \end{cases} \quad (51)$$

Equation (50) is solvable by standard methods [25]. Integral equations of the theory of radiative heat transfer have been intensively applied to diffuse cavities of simple shapes since the early 1960s. For example, Sparrow and coworkers computed the distributions of local effective emissivity for isothermal cylindrical [26] and conical [27] cavities without lids using a digital computer and method of successive approximations. Alfano [28,29] obtained analogous results for cylinders with and without a diaphragm (lid).

### 3.2.1. Zonal approximation method

When solving the integral equations discussed above inaccuracies in the calculation of the local effective emissivity can occur in cases where singularities exist. In particular, the geometry of the cavity may create singular points at the apex of a cone or at a junction of cavity walls. At some of these points, the view factors have an indeterminate form that can be evaluated with the help of L'Hôpital's rule. Kelly [30], for example, obtained the expression for the local effective emissivity of a vertex in an isothermal diffuse conical cavity:

$$\varepsilon_e(0) = \frac{\varepsilon}{\varepsilon + (1 - \varepsilon) \sin^3(\beta/2)} \quad (52)$$

where  $\beta$  is the angle at the cone vertex.

In other cases, e.g., for points lying on a junction line between the bottom and lateral wall of cylindrical cavity, the view factor is indefinite and the radiosity has a discontinuity. More importantly, the kernel in Equation (39) contains the absolute values of the difference of two homonymous coordinates (as  $|x-x'|$  or  $|x-\xi|$ ) and, correspondingly, has discontinuities in the slope (cusps) at  $x = x'$  or  $x = \xi$ . Direct application of the quadrature formulas to these points leads to inaccuracies that can only be reduced by greatly increasing the number,  $n$ , of quadrature nodes. Because the volume of computations for the iterative solution of an integral equation is proportional to  $n^2$ , the computational task grows rapidly.

Bedford and Ma [31] demonstrated that these inaccuracies cannot be completely eliminated by reasonable increasing the number of nodes in quadrature formula. To resolve this problem they proposed using the *method of zonal approximation*, which essentially transforms the integral in Equation (34) into a summation.

Following Hottel and Sarofim [4], Bedford and Ma proposed to use the zonal approximation for the integral of the form:

$$\int_0^L \varepsilon_e(\xi) dF_{x\xi} = \sum_{i=1}^n \int_{x_i}^{x_{i+1}} \varepsilon_e(\xi) dF_{x\xi} \quad (53)$$

where  $x_1 = \xi_1 = 0$ ,  $x_{n+1} = \xi_{n+1} = L$ . Assuming  $\varepsilon_e(x)$  to be a slowly varying function of  $x$ , one can write:

$$\int_0^L \varepsilon_e(\xi) dF_{x\xi} = \frac{1}{2} \sum_{i=1}^n [\varepsilon_e(\xi_{i+1}) + \varepsilon_e(\xi_i)] \int_{x_i}^{x_{i+1}} dF_{x\xi} \tag{54}$$

The integral in Equation (54) may be expressed by the difference of diffuse view factors  $F_{x\xi_i}$  and  $F_{x\xi_{i+1}}$  between an infinitesimal ring at  $\xi$  and two circular disks at  $x_i$  and  $x_{i+1}$ .

Bedford and Ma [31–34] applied the zonal approximation to diffuse isothermal and nonisothermal conical, cylindrical, cylindro-conical, double conical, and cylindro-inner-conical cavities, with and without diaphragms. Note that zonal approximation is not the only method that provides a correct solution for the Fredholm’s integral equations of the second kind with discontinuous kernels. In 1971, Yamamoto [35] used integration by parts to avoid the singularity in the equation kernel and computed the distributions of the local effective emissivity for isothermal and nonisothermal diffuse cylindrical cavities.

Chandos and Chandos [36] applied the method described in Ref. [37] in order to evaluate the integral  $\int_0^L \varepsilon_e(\xi)F(\xi, x) d\xi$ , where  $F(\xi, x)$  has a discontinuous slope at  $\xi = x$ . They used a uniform grid  $\xi_0, \xi_1, \dots, \xi_n$  on the interval  $[0, L]$  for the quadrature method. In the interval  $[\xi_{j-1}, \xi_j]$ ,  $\varepsilon_e(\xi)$  is replaced by the linear interpolation  $((\xi_j - \xi)\varepsilon_e(\xi_{j-1}) + (\xi - \xi_{j-1})\varepsilon_e(\xi_j))/(\xi_j - \xi_{j-1})$ . The integral is approximated by the sum:

$$\int_0^L \varepsilon_e(\xi)F(\xi, x) d\xi \cong \sum_{j=1}^n [\alpha_j \varepsilon_e(\xi_{j-1}) + \beta_j \varepsilon_e(\xi_j)] \tag{55}$$

where

$$\alpha_j = \frac{1}{\xi_j - \xi_{j-1}} \int_{\xi_{j-1}}^{\xi_j} (\xi_j - \xi)F(\xi, x) d\xi \tag{56}$$

and

$$\beta_j = \frac{1}{\xi_j - \xi_{j-1}} \int_{\xi_{j-1}}^{\xi_j} (\xi - \xi_{j-1})F(\xi, x) d\xi \tag{57}$$

This method was applied to the integral equations for conical, cylindrical, and extended conical (i.e., biconical) isothermal cavities and shown to have very good accuracy.

### 3.2.2. Cavities with screened walls

A geometrical shape widely used for blackbody cavities is the cylindro-inner-conical cavity (see Figure 3). A cylindro-inner-conical cavity is not a convex

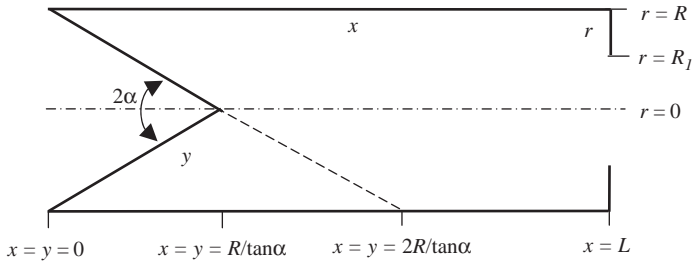


**Figure 3** Cylindro-inner-cone (from Ref. [34]).

cavity. The internal conical bottom can partially obstruct the radiation exchange between cylindrical walls, resulting in partial screening of the internal surface. Thus, there are regions inside the cylindro-inner-cone that cannot “view” one another due to screening by the reentrant cone base.

Bedford et al. studied this cavity in Ref. [34]. To simplify the analysis, they imposed the condition  $L \geq 2R/\tan \alpha$  that ensures the visibility of the entire bottom from a point on the lid and vice versa. One can write the system of integral equations for  $\varepsilon_e(x) = \varepsilon_e(x, \lambda, T_x, T_0)$ ,  $\varepsilon_e(y) = \varepsilon_e(y, \lambda, T_y, T_0)$ , and  $\varepsilon_e(r) = \varepsilon_e(r, \lambda, T_r, T_0)$ , and then apply the zonal approximation method as described above:

$$\begin{aligned}
 \varepsilon_e(x) &= \Lambda(x) + \frac{\rho}{2} \left\{ \sum_{i=1}^{n_1} [\varepsilon_e(x_{i+1}) + \varepsilon_e(x_i)] |F_{x,x_{i+1}} - F_{x,x_i}| \right. \\
 &\quad + \sum_{j=1}^n [\varepsilon_e(y_{j+1}) + \varepsilon_e(y_j)] (F_{x,y_{j+1}} - F_{x,y_j}) \\
 &\quad \left. + \sum_{k=m}^n [\varepsilon_e(r_{k+1}) + \varepsilon_e(r_k)] (F_{x,r_{k+1}} - F_{x,r_k}) \right\} \\
 \varepsilon_e(y) &= \Lambda(y) + \frac{\rho}{2} \left\{ \sum_{i=1}^{n_1} [\varepsilon_e(x_{i+1}) + \varepsilon_e(x_i)] |F_{y,x_{i+1}} - F_{y,x_i}| \right. \\
 &\quad \left. + \sum_{k=m}^n [\varepsilon_e(r_{k+1}) + \varepsilon_e(r_k)] (F_{y,r_{k+1}} - F_{y,r_k}) \right\} \\
 \varepsilon_e(r) &= \Lambda(r) + \frac{\rho}{2} \left\{ \sum_{i=1}^{n_1} [\varepsilon_e(x_{i+1}) + \varepsilon_e(x_i)] (F_{r,x_{i+1}} - F_{r,x_i}) \right. \\
 &\quad \left. + \sum_{j=1}^n [\varepsilon_e(y_{j+1}) + \varepsilon_e(y_j)] (F_{y,r_{j+1}} - F_{y,r_j}) \right\}
 \end{aligned} \tag{58}$$

Even if the condition  $L \geq 2R/\tan \alpha$  is fulfilled, mutual screening can take place for view factors  $dF_{y,x_{i+1},x_i}$ ,  $dF_{x,y_{j+1},y_j}$ , and  $dF_{x,x_{i+1},x_i}$ .

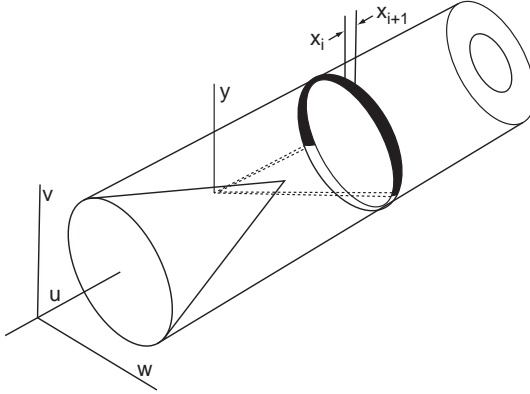


**Figure 4** For derivation of the view factor  $dF_{y,x_{i+1},x_i}$  with screening taken into account (from Ref. [32]).

Let us consider as an example the view factor  $dF_{y,x_{i+1},x_i}$  that describes the radiant transfer from the element  $dA_y$  on the conical bottom and an incomplete circular band on the cylindrical wall. Let us assume that the element  $dA_y$  of the conical surface has the coordinates  $(y, R - y \tan \alpha, 0)$  as shown in Figure 4. When  $x_{i+1} < 2R/\tan \alpha$ ,  $dF_{y,x_{i+1},x_i}$  can be expressed as the absolute value of the difference in view factors between  $dA_y$  and circular segments defined by  $x_i$  and  $x_{i+1}$ :

$$dF_{y,x_{i+1},x_i} = |F_{y,x_i} - F_{y,x_{i+1}}| \quad (59)$$

The view factor  $dF_{y,x_i}$  can be evaluated using Stokes theorem which converts the double integral over the area of the segment at  $x_i$  to the sum of three single contour integrals around the boundary of the segment (see Ref. [1], pp. 128–136). For the local coordinate system,  $(u, v, w)$  chosen in such a way that one of the three integrals becomes zero, and the other two correspond to each part of the two-part boundary:

$$\begin{aligned} F_{y,x_i} = & \frac{\sin \alpha}{2\pi} \left\{ \phi(x_i) + \frac{2(2R^2 - a_i)}{\sqrt{a_i^2 - b^2}} \tan^{-1} \left[ \frac{\sqrt{a_i^2 - b^2}}{a_i + b} \tan \frac{\phi(x_i)}{2} \right] \right\} \\ & + \frac{1}{\pi} \tan^{-1} \left[ \frac{R \sin \phi(x_i)}{(x_i - y) \sec \alpha} \right] \\ & + \frac{(x_i - y) \cos \alpha}{2\pi(R - y \tan \alpha)} \left\{ \phi(x_i) - \frac{2a_i}{\sqrt{a_i^2 - b^2}} \tan^{-1} \left[ \frac{\sqrt{a_i^2 - b^2}}{a_i + b} \tan \frac{\phi(x_i)}{2} \right] \right\} \end{aligned} \quad (60)$$

where

$$\begin{aligned}\phi(x_i) &= \cos^{-1}\left(1 - \frac{x_i \tan\alpha}{R}\right) \\ a_i &= R^2 + (x_i - \gamma)^2 + (R - \gamma \tan\alpha)^2 \\ b &= -2R(R - \gamma \tan\alpha)\end{aligned}\quad (61)$$

If  $x_i > 2R/\tan\alpha$ , there is no screening, and the circular segments become complete circular disks. Then the expression for  $dF_{\gamma, x_i}$  reduces to

$$F_{\gamma, x_i} = \frac{\sin\alpha}{2} \left[ 1 - \frac{a_i - 2R^2}{\sqrt{a_i^2 - b^2}} \right] + \frac{(x_i - \gamma) \cos\alpha}{2(R - \gamma \tan\alpha)} \left[ 1 - \frac{a_i}{\sqrt{a_i^2 - b^2}} \right] \quad (62)$$

To derive the remaining view factors in Equations (58) and treat their singularities, the same approach as described in Refs. [31–33] is applied.

Meier et al. [38] examined a spherical cavity with a cylindrical extension. Such a cavity has the mutually screened regions of the internal surface: if the radius of the cylinder is less than that of the sphere, the spherical part of the cavity may not be completely visible from a point on its cylindrical part. They composed a system of the integral equations and derived the necessary expressions for view factors. However, the authors of Ref. [38] were apparently unacquainted with Ref. [34], since the solution for the effective emissivity was only determined in first approximation of a power series expansion. Nevertheless, since the authors of Ref. [38] only examined the quality of a cylindrical–spherical cavity with an internal coating of very high emissivity ( $\varepsilon \geq 0.95$ ), the first-approximation solution was sufficient.

### 3.3. Integrated effective emissivity of diffuse cavities

The method of integral equations for diffuse cavities enables the calculation of the distributions of the local effective emissivity over the internal surface of a cavity. In practice, however, it is necessary to know the values of effective emissivity that correspond to the specific arrangement of the cavity and the detector. These values can be obtained by integrating the distribution of the local effective emissivity over the area of visibility.

Let us consider two diffuse cavities of arbitrary shape, the same depth  $L$ , and reference temperature  $T_0$ , with no internal screening, and a coaxial circular detector of radius  $R_d$ , spaced at a distance  $H$  from the cavity aperture (Figure 5). The principal distinction between the two systems depicted in Figure 5 is the difference in the visibility of the internal cavity surface from any point on the detector. For a cavity without a lid, the entire internal surface can be observed from any point on the detector. Thus, the

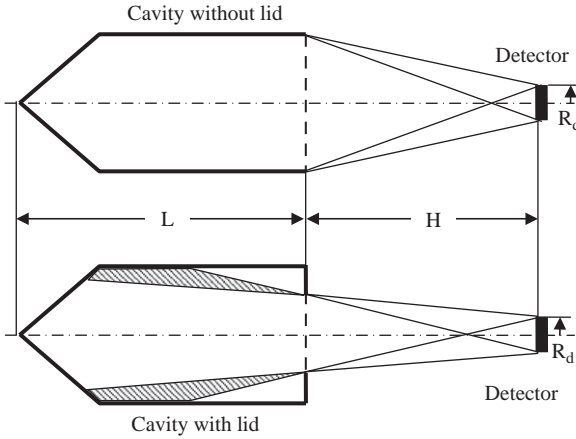


**Figure 5** Cavity-detector systems with (lower) and without (upper) vignetting.

radiation flux falling onto the detector is equal to

$$\Phi = M_{\text{bb}}(T_0) \int_0^L \varepsilon_c(x, T_0) F_{\text{xd}}(L + H - x) dA_x \quad (63)$$

where  $M_{\text{bb}}$  is the radiant exitance of a blackbody (in  $\text{W}/\text{m}^2$ ) and  $F_{\text{xd}}(x)$  is the view factor between the annular element  $dA_x$  of the cavity surface placed at a distance  $x$  from the bottom vertex and the detector. According to the integrated emissivity definition (10),

$$\begin{aligned} \varepsilon_{\text{e,c}}(H, T_0) &= \frac{\int_0^L \varepsilon_c(x, T_0) F_{\text{xd}}(L + H - x) dA_x}{\int_0^L F_{\text{xd}}(L + H - x) dA_x} \\ &= \frac{1}{F_{\text{dd}}(H)} \int_0^L \varepsilon_c(x, T_0) F_{\text{xd}}(L + H - x) dA_x \end{aligned} \quad (64)$$

where  $F_{\text{dd}}$  is the view factor from the cavity aperture to the detector (view factor between two coaxial disks).

Sparrow and Heinisch [39] computed the hemispherical ( $H=0$ ) effective emissivity and examined the dependence of the integrated effective emissivity on  $H$  and  $R_d$  for a cylindrical cavity without a lid. They found that the distance between the detector and the cavity aperture plays an important role on the normal effective emissivity results, and that the detector radius is only of secondary importance. Furthermore, the normal effective emissivity exceeds the hemispherical effective emissivity for cavities having a depth-to-radius ratio greater than unity. Alfano and Sarnö [40] expanded the analysis to baffled cylindrical cavities but assumed that the detector was infinitesimal.

For a baffled cavity, there are three zones on its internal surface (see lower part of Figure 5): one that is visible from every point on the detector; the other that is invisible from any point on the detector; and the third that is a zone of penumbra (shaded area in Figure 5) where the visibility depends on the positions of both the location on the cavity and the location on the detector.

The size of the penumbra region decreases when  $H$  increases. Thus, the influence of the vignetting effect on the integrated effective emissivity can be neglected for an infinitely distant detector (i.e., for the normal effective emissivity) because all of the rays falling onto detector are parallel to the cavity axis.

A double integration with variable integral terms was applied in Ref. [41] to obtain rigorous solutions for the baffled conical and cylindrical cavities. This method was generalized in Ref. [42] for the precise evaluation of the integrated effective emissivity of any practical cavity with circular symmetry.

An alternative approach to the view factors calculation based on the Stokes's theorem and contour integration was proposed in Ref. [43]. In this approach, the triple numerical integration is replaced by a single integration, which, in turn, is replaced by a zonal summing approximation. The authors of Ref. [43] considered a diffuse frustum cone with a reentrant cone base and an optional stop of radius  $R_0$  between the cavity aperture and the detector. The authors indicated that the computing time was substantially reduced and the precision of the integrated emissivity calculation was increased as compared to the conventional formulation.

### 3.4. Series technique for multiple reflections in cavities

#### 3.4.1. Diffuse cavities

Ohwada in Ref. [23] described a method for calculating the effective emissivity of diffuse cavities that is based on iterative solution of the integral equations of the form of Equation (40). The main equation of this method is like Equation (43) which links an  $n$ th approximation to those of orders  $n-1$  and  $n-2$ . Ohwada referred to her method as a *series technique* (see Refs. [44,45]). In the numerical solution of the integral equations, the zonal approximation method [31] was employed for view factors. Ohwada applied this technique to the calculation of the local effective emissivities of isothermal cylindrical [46], conical [44], cylindro-conical and double conical cavities [45], as well as their integrated effective emissivities [47]. In Refs. [48,49], this technique was extended to the spectral, total, and band-limited effective emissivities of nonisothermal cavities of various geometrical shapes. Ohwada and Sakate also calculated effective emissivities for a cylindrical cavity with a longitudinal strip opening [50].

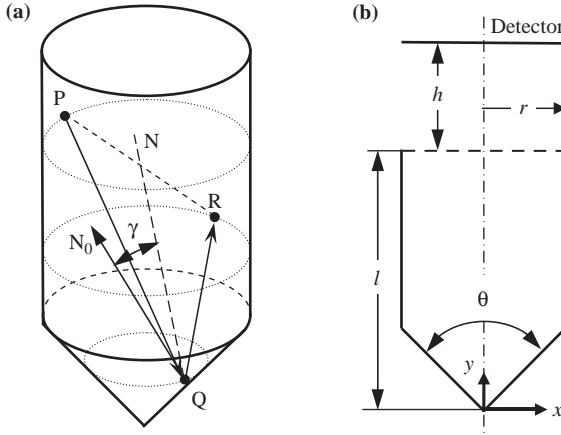


**Figure 6** (a) Schematic illustration of incident and reflected rays, and angle  $\gamma$ . (b) Geometry of the cavity and the detector (from Ref. [51], with alterations).

### 3.4.2. Non-Lambertian cavities

Ohwada in Ref. [51] attempted to extend the series technique to cavities with non-Lambertian internal walls. The positions  $Q$  and  $P$  in Figure 6(a) are on the cavity wall and point  $R$  is on the cavity wall or on the cavity opening.

Area elements located at  $P$ ,  $Q$ , and  $R$  are denoted by  $\Delta_P$ ,  $\Delta_Q$ , and  $\Delta_R$ , respectively. Radiation leaves  $\Delta_P$ , falls on  $\Delta_Q$ , and after undergoing a reflection, falls on  $\Delta_R$ . The number of the area elements on the cavity wall is given by  $k$ , while the total number of area elements on the cavity wall and opening is given by  $m$ . The direction from  $Q$  to  $R$  is designated  $\Psi_{QR}$ . The radiance of  $\Delta_Q$  in the direction  $\Psi_{QR}$  is designated  $L(Q, \Psi_{QR})$ . Then

$$L_n(Q, \Psi_{QR}) = L_{n-1}(Q, \Psi_{QR}) + \sum_{P=1}^k f(\Psi_{QP}, \Psi_{QR}) [L_{n-1}(Q_P, \Psi_{PQ}) - L_{n-2}(Q_P, \Psi_{PQ})] \cos(\phi_{QP}) \Delta\omega_{QP} \quad (65)$$

where

$$L_0(Q, \Psi_{QR}) = 0 \quad (66)$$

$$L_1(Q, \Psi_{QR}) = \varepsilon_0 L_B(T) \quad \text{for } Q = 1, 2, \dots, k; \quad R = 1, 2, \dots, k, \dots, m \quad (67)$$

where  $\Psi_{QP}$  is the direction from  $Q$  to  $P$ ,  $\phi_{QP}$  the angle between the normal  $QN_0$  to  $\Delta_Q$  and the line connecting  $Q$  and  $P$ ,  $\Delta\omega_{QP}$  the solid angle subtended by  $P$  when viewed from a point  $Q$ ,  $L$  the radiance of the cavity wall at temperature  $T$ , and  $\varepsilon_0$  is the surface emissivity, assumed to be independent of the direction for simplicity.

To simulate a non-Lambertian surface, the angle  $\gamma$  between the normal  $QN_0$  and the line  $QN$ , bisecting  $\angle PQR$ , is introduced. The bidirectional reflectance distribution function (BRDF), in accordance with its definition [10] is expressed as follows:

$$f(\Psi_{QP}, \Psi_{QR}) = \frac{\rho_0 g[\gamma(\Psi_{QP}, \Psi_{QR})]}{\sum_{R=1}^m g[\gamma(\Psi_{QP}, \Psi_{QR})] \cos(\phi_{QR}) \Delta\omega_{QR}} \quad (68)$$

where  $\phi_{QR}$  is the reflection angle,  $\rho_0 = 1 - \varepsilon_0$  the directional-hemispherical reflectance, and

$$g[\gamma(\Psi_{QP}, \Psi_{QR})] = \exp[-a\gamma^2(\Psi_{QP}, \Psi_{QR})] \quad (69)$$

Such a Gaussian dependence of the BRDF on the angle  $\gamma$  can be used for approximate description of optical properties of randomly rough surfaces. When  $a = 0$ , the BRDF is Lambertian. When  $a \rightarrow \infty$ , the reflection is specular.

The integrated effective emissivity for the detector arrangement shown in Figure 6(b) is calculated according to the following equation:

$$\varepsilon_{e,c} = \frac{\sum_Q \sum_R L(Q, \Psi_{QR}) \cos(\phi_{QR}) \Delta\omega_{QR} \Delta\omega_{QL}}{L_B(T) \sum_Q \sum_R \cos(\phi_{QR}) \Delta\omega_{QR} \Delta\omega_{QL}} \quad (70)$$

where  $L(T)$  is the radiance of a black body at temperature  $T$  of the cavity surface. The summations are carried out over the ranges of  $Q$  and  $R$ . Radiation leaving  $\Delta_Q$  in the direction of  $\Psi_{QR}$  arrives at the detector. The dependences of  $\varepsilon_{e,c}$  upon various geometrical parameters was computed and compared with that for a Lambertian reflection [51].

However, results of calculations performed for a closed cavity (perfect blackbody) have a deviation in effective emissivity from unity of up to 0.01. In Ref. [51], Ohwada supposed that the calculation accuracy might be improved by subdividing the cavity surface into a finer mesh and increasing the number of significant digits for computing the quantities related to the geometric factors. In her subsequent paper [52], Ohwada concluded that the reason for the poor accuracy in her calculation was due to an intrinsic contradiction in the model related to the optical properties of the cavity wall. The integration of the BRDF containing the Gaussian factor as in Equation (69) over the entire hemispherical range of viewing directions results in a directional-hemispherical reflectance that depends on incident angle. According to Kirchhoff's law, the emissivity of such a surface must also depend on the emission angle. However, in Ref. [51], the angular independence of  $\rho_0$  and  $\varepsilon_0$  was assumed.

This was improved in Ref. [52] by using the reciprocity rule and considering  $\rho_0$  and  $\varepsilon_0$  as functions of the incident angle for several more

realistic models of the BRDF. These improvements were implemented and the deviations of effective emissivity from unity for a closed cavity were reduced to values less than the truncation error (about  $10^{-4}$ ); the hemispherical, normal, and integrated emissivities for a coaxial detector, and for a detector with optical system consisting of a lens and two stops were computed, and the influence of the surface condition (i.e., of the parameter  $a$ ) on these values was investigated.

### 3.5. Cavities with diffusely emitting and specularly reflecting walls

In the infrared spectral range, when the surface roughness becomes negligible in comparison with the wavelength of the incident radiation, the diffuse model cannot adequately describe the optical properties of surfaces such as polished and oxidized metals, and other materials with significant surface (i.e., not volumetric) reflection. For this case, a model that incorporates diffuse thermal emission and specular reflection is more suitable. The calculation of the effective emissivity for these cavities is greatly simplified. The problem is reduced to ray tracing and multiplication of the radiance by  $\rho$ , after each reflection. According to Kirchhoff's law, the local directional effective emissivity is given by

$$\varepsilon_e(x, \theta, \phi) = 1 - \rho_e(\text{aperture}, \theta, \phi, 2\pi) \quad (71)$$

where  $\rho_e(\text{aperture}, \theta, \phi, 2\pi) = \rho^{n(\theta, \phi)}$  is the effective reflectivity of the cavity and  $n(\theta, \phi)$  is the number of reflections undergone by a ray falling from the direction  $(\theta, \phi)$  before it is reflected out of the aperture in any direction.

The most common geometry for a cavity with specularly reflecting walls is a cone. For a ray entering a cone at an oblique angle  $\psi$  and striking the surface at an angle  $\gamma$  to the generatrix of the cone, the number of reflections occurring before the ray finally leaves the cone is [53]

$$n = \text{Ent} \left( \frac{\pi - 2\gamma + 2\alpha \cos\psi}{2\alpha \cos\psi} \right) \quad (72)$$

where  $\alpha$  is the cone apex half-angle and  $\text{Ent}(x)$  represents the greatest integer which is less than or equal to  $x$ .

Equation (72) shows that it is preferable to view a specular cone at an oblique angle rather than axially. The practical limit to  $n$  is set by the width of the beam, since  $\psi$  varies over the width due to the curvature of a conical surface. The presence of even a small fraction of diffuse reflection can significantly decrease the effective emissivity of a specularly reflecting conical cavity.

The analytical approach becomes increasingly complicated, if one or more of the surfaces inside a cavity reflect thermal radiation diffusely. In Ref. [54], a cylindro-inner-conical cavity with a specularly reflecting flat lid

is considered. The authors used Stokes theorem to reduce the double integrals to a single contour integral around a finite area on the specular lid and the exchange factors developed in Ref. [55]. The general form of the exchange factor is

$$dE_{x_i, x_j} = \sum_{n=0}^{\infty} (\rho_m)^n df_n \quad (73)$$

where  $x_i$  is the position of an emitting element  $dA_i$ ,  $x_j$  the position of a receiving element  $dA_j$ ,  $\rho_m$  the specular reflectance of the lid, and  $df_n$  the fraction of diffusely distributed radiative flux from  $dA_i$  that arrives at  $dA_j$  with  $n$  intervening ideal (i.e., with  $\rho_m = 1$ ) specular reflections.

The authors of Ref. [54] found that the distributions of the effective emissivity over the internal surface of a cavity with a specular lid are very close to those in the similar purely diffuse cavity (see Ref. [34]).

### 3.6. Specular–diffuse cavities

According to the specular–diffuse (SD) model of reflection (e.g., see Chapter 5 of Ref. [1]), the directional-hemispherical reflectance  $\rho$  is represented by the sum of diffuse and specular components  $\rho_d$  and  $\rho_s$ , respectively. It is supposed that  $\rho$ ,  $\rho_d$ , and  $\rho_s$  do not depend on incident angle. The differential exchange factor  $dE_{dA, dA'}$ , which replaces the view factor in diffuse–specular enclosures, is defined as the sum of fractions of diffuse radiation leaving  $dA$  that arrives at  $dA'$  both directly and after all possible specular reflections. Analytical derivation of the exchange factors can be a very laborious process. Hence, the integral equations method is rarely applied to specular–diffuse cavities.

However, Kowsary and Mahan in Ref. [56] used the integral equation method for calculating the effective emissivity of a specular–diffuse spherical cavity with an isothermal surface. They calculated the hemispherical effective emissivity of the specular–diffuse spherical cavity against the opening half-angle for various values of the ratio  $\rho_s/\rho$ .

### 3.7. Method of successive reflections

De Vos [57] considered a cavity (see Figure 7) with opaque walls and one opening. One can express the spectral radiation flux emitted by a surface element  $dw$  in the direction  $\mathcal{G}_w^o$  within the solid angle  $d\Omega_w^o$  and for the temperature  $T$ , as

$$\varepsilon_w^o I_B dw \cos \mathcal{G}_w^o d\Omega_w^o \quad (74)$$

where  $I_B$  is the radiant intensity of a blackbody at a temperature  $T$ ,  $\varepsilon_w^o$  the hemispherical emissivity of  $dw$  at temperature  $T$  in the direction  $\mathcal{G}_w^o$ , and  $d\Omega_w^o$  the solid angle subtended by  $do$  when viewed from  $dw$ .

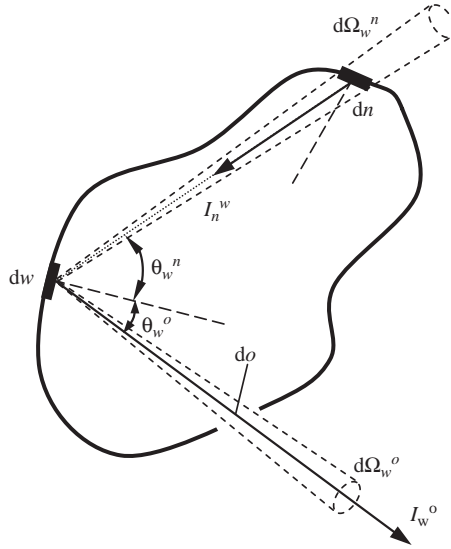


**Figure 7** Blackbody cavity with one opening,  $dw$  and  $dn$  are the elements of the cavity inner surface,  $do$  is an element of the cavity opening (from Ref. [57]).

The spectral radiation flux coming from a given surface element  $dn$  and reflected by  $dw$  into the solid angle  $d\Omega_w^o$  is given by

$$I_n^w d\Omega_w^n dw \cos\vartheta_w^n r_w^{no} d\Omega_w^o \tag{75}$$

where  $I_n^w$  is the radiant intensity of  $dn$  in the direction of  $dw$  at a temperature  $T$ ,  $d\Omega_w^n$  the solid angle subtended by  $dn$  when viewed from  $dw$ ,  $d\Omega_w^o$  the solid angle subtended by  $do$  when viewed from  $dw$ , and  $r_w^{no}$  the partial reflectivity of  $dw$  at temperature  $T$  for the direction from  $dn$  to  $do$ .

The *partial reflectivity*,  $r_x^{ab}$  (the quantity used by De Vos), of the surface element  $dx$  is the fraction of the radiation reflected in the direction  $b$  per unit solid angle when the radiation is incident from the direction  $a$ . From this definition, it follows that the directional-hemispherical reflectivity for radiation falling from the direction  $a$  is

$$\rho^a = \int_{2\pi} r^{an} d\Omega^n \tag{76}$$

where  $d\Omega^n$  is the solid angle in a direction  $n$  and  $r^{an}$  is the partial reflectivity in this direction.

The integration is performed over the hemispherical solid angle. The Helmholtz' theorem of reciprocity can be written for the partial reflectivities:

$$r^{ab} \cos\vartheta^a = r^{ba} \cos\vartheta^b \tag{77}$$

The relationship linking the De Vos's partial reflectivity with the BRDF (see Ref. [10]) is

$$\frac{r^{ab}}{\cos\theta^b} = f_r(a, b) \quad (78)$$

The first-order approximation for  $I_n^w$  is

$$I_n^w = I_B \left( 1 - \sum_h r_n^{wh} d\Omega_n^h - k_n \varepsilon_n^w \right) \quad (79)$$

where  $\varepsilon_n^w$  is the emissivity of  $dn$  at temperature  $T_n$ , in the direction of  $dw$ ,

$$k_n = \frac{I_B(T) - I_B(T_n)}{I_B(T)} \quad (80)$$

The second-order approximation for  $I_w^o$  is given by

$$I_w^o = I_B \left( 1 - \sum_h r_w^{oh} d\Omega_w^h - \sum_h \int r_n^{wh} d\Omega_n^h r_w^{on} d\Omega_w^n - \int k_n \varepsilon_n^w r_w^{on} d\Omega_w^n \right) \quad (81)$$

The integration is to be extended over the entire surface (except the opening). In the third-order approximation, terms containing the product of three partial reflectivities and three solid angles must be added to Equation (81). In principle, the method described enables the calculation of the directional effective emissivity for cavities whose walls have arbitrary BRDFs (or partial reflectivities). Usually, however, less complicated and more idealized models of reflection are employed (e.g., purely diffuse, purely specular, or mixed, SD models).

Campanaro and Ricolfi in Ref. [58] used De Vos's method for calculating the effective emissivity of an isothermal specular–diffuse sphere. Using a third-order approximation, they showed that the effective emissivity decreases as the specular component is increased. The same authors in Ref. [59] applied De Vos's technique to the computation of the total effective emissivity of a nonisothermal spherical cavity with a diffusely emitting and reflecting internal surface. An analytical solution was derived for the general temperature distribution case. Assuming a linear temperature gradient along the axis normal to the opening, the authors obtained numerical dependences for various values of the ratio of the opening radius to the sphere radius.

Quinn [60] applied De Vos's method to an isothermal diffuse cylindrical cavity with and without a diaphragm. For the open-ended cylinder, Quinn obtained a second-order approximation for the effective emissivity of the bottom center:

$$\varepsilon_c = 1 - \frac{\rho}{D^2} - \rho^2 I_2 \quad (82)$$

where  $D$  is the length of the cylinder of unit radius, and

$$I_2 = \frac{1}{\pi} \int_0^D \int_{-\pi/2}^{\pi/2} \frac{D-x}{[1+(D-x)^2]^2} \left[ \tan^{-1} \left( \frac{2\cos\phi}{x} \right) - \frac{2x\cos\phi}{x^2+4\cos^2\phi} \right] d\phi dx \quad (83)$$

For the lidded cylinder, Quinn found that

$$\varepsilon_e = 1 - \frac{\rho a^2}{D^2} - \rho a^2 I'_2 \quad (84)$$

where  $a$  is the dimensionless radius of the aperture,

$$I'_2 = 2 \int_0^D \frac{x(D-x)}{(1+x^2)^2[1+(D-x)^2]^2} dx \quad (85)$$

The integrals  $I_2$  and  $I'_2$  were evaluated numerically, for  $D$  ranging from 4 to 20 and tabulated.

Quinn and Martin [61] investigated the radiation heat transfer from a blackbody cavity radiator to an absolute cavity detector. Both cavities have the shape of a cylinder-inner cone and coated inside with black paint. The paint has a specular component of reflection that increases with wavelength and incident angle. A second-order approximation was used. Terms of higher order were taken into account by summation of all reflections starting from the third, but were found to be negligible.

In Ref. [62], Berry applied a second-order approximation of De Vos's method to the isothermal diffuse cylinder-inner-cone (cylinder with a reentrant cone). Redgrove and Berry [63] used De Vos's approach to compute the effective emissivity of the same cavity but with a specular-diffuse reflection from the internal surface. They analyzed the dependences of the effective emissivity on the geometrical parameters of a cavity, the emissivity of the wall, and the ratio  $\rho_s/\rho$ . A correction term for nonisothermal conditions to the total effective emissivity was also derived. The difficulty of analytical integration, as well as the accumulation of truncation errors due to the numerical calculation of nested integrals, restricted the number of reflections that could be considered to two. This limitation can lead to significant errors in calculating the effective emissivity for a cavity with even moderately low values of wall emissivity.

## 4. MONTE CARLO METHOD

### 4.1. Stochastic approach to radiative heat transfer

The Monte Carlo method is a class of numerical techniques based on the implementation of a stochastic model to an object under consideration in

order to evaluate its characteristics on the basis of the law of large numbers. Several excellent monographs [64–69] cover the basics of various Monte Carlo methods including time-saving algorithms, methods of convergence acceleration, etc. Because of their reliance on repeated computation and random or pseudorandom numbers, Monte Carlo methods are best suited to calculation by a computer and are used when it is impossible or impractical to compute an exact result with a deterministic algorithm.

Physicists working on the Manhattan Project at Los Alamos National Laboratory originally coined the term *Monte Carlo* in the 1940s [70]. It is named after the famous gambling casino in Monaco because the method is analogous to the random and repetitive processes common in gambling. Initially, the Monte Carlo method was applied to studying neutron interactions with matter. Monte Carlo's probabilistic treatment of the radiation–matter interaction effects is well suited to solving computational problems concerning atmosphere optics [71], radiative heat exchange [72,73], computer graphics [74–77], remote sensing, infrared scene and target simulation, etc.

When we consider optical radiation transfer problems within the framework of geometric optics, the application of the Monte Carlo method is a conceptual process performed by a computer in which a *particle* (sometimes referred to as a *bunch*, or *bundle of particles* or even *of rays*) starts from a point on a surface and moves away from the surface in a random direction. Frequently, the term *photons* is used for such particles; however, real photons have nothing physically in common with the particles of such a model. The number of particles moving in each of a finite (but very large) number of directions is defined by a solid angle and each is weighted to match the angular distribution of radiation flux. After a sufficiently large number of particles have been traced from the source to the receiver by this process (the limit is determined by computer performance and the investigator's accuracy requirements), the process is terminated and the fraction of particles reaching a receiver from the source is determined. Since the energy content of each particle is known, the flux falling on the receiving surface can easily be determined.

In real situations, an intermediate surface may interact with the radiation resulting in partial reflection, absorption, or transmission by that surface. Any reflected radiation can propagate according to its own distribution of reflected radiance where it can be partially reflected again. In general, there are an infinite number of multiple reflections between two mutually irradiating surfaces, and the Monte Carlo approach easily accommodates this situation.

In a computer stochastic model, the actual distributions of radiation fluxes over spatial and angular domains are replaced with probability density functions (PDF) for the appropriate random variates. Effective computer modeling of these random variates is the most important component of the

Monte Carlo method. Modeling an arbitrary PDF is usually based on a pseudorandom number generator (PRNG) – a computer program that produces a sequence of floating-point numbers uniformly distributed on the  $[0, 1)$  interval (see Ref. [78]). Often the correctness and the precision of the modeling depend on the quality of these random sequences. A PRNG designed for critical modeling programs must undergo a thorough examination of periodicity, multidimensional equidistribution, various statistical tests of distribution uniformity, etc. [79]. Recent investigations show that most widely used PRNG have serious defects [80]. On the basis of their own experience, the authors of Ref. [81] recommend the Mersenne–Twister PRNG [82], which provides an extremely large period of  $2^{19937} - 1$  and up to 623-dimensional equidistribution for 32-bit accuracy. The Mersenne–Twister PRNG is freely distributed software. Recent versions of the code for its algorithm are available on the web (see Ref. [83]).

The computational problem that is usually solved by the Monte Carlo method concerns the evaluation of the mean value of a random variate. The random uncertainty of such an estimate decreases as  $N^{-1/2}$  ( $N$  is the number of random trials) and does not depend on the dimension of the problem solved.

For radiative transfer inside cavities, the dimension of the estimated random variate is the maximum number of consecutive reflections that a ray undergoes until it escapes the cavity. It is sufficient to compare this with the method of successive reflections, described earlier where the precision of the results decreases due to accumulations of the truncation errors at the computation of nested integrals, to understand the advantages of the Monte Carlo method.

## 4.2. Ray tracing

Instead of a particle or a bunch, or bundle of particles, we shall refer hereinafter to the rays traced inside a cavity in keeping with the terminology used in ray or geometric optics. Each of the  $n$  surfaces that form a cavity can be described in terms of the Cartesian coordinate system as

$$\Phi_i(x, y, z) = 0, \quad i = 1, 2, \dots, n \quad (86)$$

The parametric equations of a ray in Cartesian coordinates are:

$$\begin{cases} x = x' + \omega_x t \\ y = y' + \omega_y t \\ z = z' + \omega_z t \end{cases} \quad (87)$$

where  $(x', y', z')$  and  $(x, y, z)$  are the coordinates of the start and end points of a ray, respectively,  $(\omega_x, \omega_y, \omega_z)$  are the coordinates of a unit vector  $\boldsymbol{\omega}$  of

a ray direction, and  $t$  is a time-like parameter. First Equations (86) and (87) are solved together to obtain the parameters  $t_i$  for each  $i$ . Once a minimal positive  $t$  is found, then we can determine the coordinates  $(x, y, z)$  using Equation (87).

There are several books devoted to ray tracing in computer graphics [75,77,84]. They contain efficient algorithms for determining the intersection points of a ray with the surfaces of common cavity structures.

### 4.3. Stochastic models for optical properties

The optical properties of a surface can be exhaustively described by the spectral BRDF [10]:

$$f(\lambda, \theta_i, \phi_i, \theta_r, \phi_r) = \frac{dL_{\lambda,r}(\lambda, \theta_r, \phi_r)}{dE_{\lambda,i}(\lambda, \theta_i, \phi_i)} \quad (88)$$

where  $L_{\lambda,r}$  is the spectral radiance of reflected radiation,  $E_{\lambda,i}$  the spectral irradiance (in  $\text{W}/\text{m}^2$ ) from incident radiation, and  $(\theta_i, \phi_i)$  and  $(\theta_r, \phi_r)$  are the directions of incidence and observation, respectively, defined by their spherical coordinates.

In the case of unpolarized optical radiation, the BRDF is a function of five arguments. Usually, experimental data exist only for several wavelengths, and angular scanning is performed in the plane of incidence. This is why it is often impossible to directly use the measured BRDF in the Monte Carlo algorithms. Therefore, it is necessary to have a reliable model of the BRDF that satisfies the experimental data and predicts physically plausible values for the BRDF for the complete range of arguments where there is a lack of experimental data. The model of BRDF must obey the energy conservation law:

$$\rho(\lambda, \theta_i, \phi_i, 2\pi) = \int_{\phi_r=0}^{2\pi} \int_{\theta_r=0}^{\pi/2} f(\lambda, \theta_i, \phi_i, \theta_r, \phi_r) \sin\theta_r \cos\theta_r \, d\theta_r \, d\phi_r \leq 1 \quad (89)$$

where  $\rho(\lambda, \theta_i, \phi_i, 2\pi)$  is the spectral directional-hemispherical reflectance. The spectral directional emissivity of an opaque body is equal to

$$\varepsilon(\lambda, \theta_i, \phi_i) = 1 - \rho(\lambda, \theta_i, \phi_i, 2\pi) \quad (90)$$

The model of BRDF should also be consistent with the reciprocity principle:

$$f(\lambda, \theta_i, \phi_i, \theta_r, \phi_r) = f(\lambda, \theta_r, \phi_r, \theta_i, \phi_i) \quad (91)$$

If the angular distribution of the emitted or reflected radiant intensity is known, it is possible to construct a simple stochastic model by generating random rays, which are uniformly distributed in a hemisphere, and assigning to each ray a statistical weight proportional to the radiant intensity

in that direction. However, such a model is computationally inefficient, especially for BRDF with significant nonuniformities. For more effective modeling, the stochastic model of BRDF, which is incorporated into a Monte Carlo ray-tracing algorithm, should provide importance sampling [85]. In other words, random directions of reflection  $(\theta_r, \phi_r)$  should be generated from a general population that has a PDF equal to  $f(\lambda, \theta_i, \phi_i, \theta_r, \phi_r) \cos(\theta_r)$ .

## 4.4. Monte Carlo modeling of specular–diffuse blackbodies

### 4.4.1. Early Monte Carlo studies

Polgar and Howell [86] applied the Monte Carlo method to the stochastic modeling of the reflective properties of a diffuse conical cavity irradiated by collimated radiation. Corlett [87] described in detail a modeling algorithm for the thermal radiation exchange among opaque specular–diffuse surfaces separated by vacuum. The algorithm developed was applied to the calculation of radiative heat transfer from one surface to another in a closed specular–diffuse cavity. Random numbers  $u$  uniformly distributed on the segment  $(0, 1]$  were employed in the following cases:

- (i) to choose between reflection and absorption: absorption, if  $u_\alpha < \alpha$ , where  $\alpha$  is a surface absorptance, and reflection otherwise;
- (ii) to choose between specular and diffuse reflection: specular, if  $u_s < \rho_s/\rho$ , where  $\rho_s$  is the specular component of the directional-hemispherical reflectance  $\rho$ , and diffuse otherwise;
- (iii) to generate a direction  $(\theta, \phi)$  of diffuse reflection: in the local spherical coordinate system,

$$\cos\theta = \sqrt{u_\theta}, \quad \phi = 2\pi u_\phi$$

Toor and Viskanta [88] investigated the precision of their Monte Carlo calculations against known analytical solutions for specular–diffuse surfaces. They also considered directional-dependent specular reflection, which is predicted from Fresnel's equations in terms of the complex index of refraction  $\tilde{n}(\lambda) = n(\lambda) - ik(\lambda)$ . In addition, they calculated the BRDF  $f(\lambda, \theta_i, \phi_i, \theta_r, \phi_r)$ , which was approximated by

$$f(\lambda, \theta_i, \phi_i, \theta_r, \phi_r) \approx \rho(\lambda, \theta_i) f_\infty(\lambda, \theta_i, \phi_i, \theta_r, \phi_r) \quad (92)$$

where  $f_\infty(\lambda, \theta_i, \phi_i, \theta_r, \phi_r)$  is Beckmann's reflection distribution function for a perfect conductor (Beckmann's solution [89] is based on Kirchhoff's approximation of diffraction integrals; it satisfies reciprocity but violates energy conservation due to neglecting multiple reflections). The function  $f_\infty$  also depends upon parameters of surface roughness.

To implement the importance sampling (i.e., to generate the random directions of reflection according to the BRDF), Toor and Viskanta

employed the inverse transform of cumulative distribution function. For polar and azimuthal angles, cumulative distribution function can be written as

$$R_{\theta_r}(\lambda, \theta_i, \phi_i) = \frac{\int_0^{\theta_r} \int_0^{2\pi} f(\lambda, \theta_i, \phi_i, \theta_r, \phi_r) \cos\theta_r \sin\theta_r d\phi_r d\theta_r}{\int_0^{\pi/2} \int_0^{2\pi} f(\lambda, \theta_i, \phi_i, \theta_r, \phi_r) \cos\theta_r \sin\theta_r d\phi_r d\theta_r} \quad (93)$$

and

$$R_{\phi_r}(\lambda, \theta_i, \phi_i) = \frac{\int_0^{\pi/2} \int_0^{\phi_r} f(\lambda, \theta_i, \phi_i, \theta_r, \phi_r) \cos\theta_r \sin\theta_r d\phi_r d\theta_r}{\int_0^{\pi/2} \int_0^{2\pi} f(\lambda, \theta_i, \phi_i, \theta_r, \phi_r) \cos\theta_r \sin\theta_r d\phi_r d\theta_r} \quad (94)$$

The values of  $\theta$  versus  $R_\theta$  and  $\phi$  versus  $R_\phi$  were calculated and stored in computer memory for each angle of incidence  $\theta_i$  with the increments of  $5^\circ$ . From this table the direction of the reflection  $(\theta_r, \phi_r)$ , corresponding to a given angle of incidence  $\theta_i$ , was obtained by interpolation.

Although Refs. [86–88] are not directly devoted to the radiative properties of blackbody radiators, they showed the applicability of the Monte Carlo method to the calculation of the effective emissivity of blackbody radiators and demonstrated the possibilities of using the stochastic approach to the modeling of radiation heat transfer.

#### 4.4.2. Hemispherical effective emissivity of diffuse cavities

Sparrow and coworkers in a series of publications [90–92], proposed a method of variance reduction in the Monte Carlo modeling of the radiative properties of a diffuse cavity which they called *energy partitioning*. They applied it to isothermal baffled conical and cylindrical cavities. The essence of the method is the following. A random point on a radiating surface of a cavity emits a ray. Let  $F$  represent the fraction of the radiation emitted at that point, which passes directly out of the aperture, that is, the diffuse view factor of the aperture from that point. The energy content  $E^*$  of the  $i$ th ray is partitioned into two portions. One portion,  $F_i E^*$ , passes directly out of the aperture and is tallied. The other portion,  $(1-F_i)E^*$ , remains within the cavity and is carried by the ray along a straight path. Before the trajectory of the ray is traced, a random number  $R_\alpha$ , having a value between 0 and 1, is selected to determine whether or not the ray will be absorbed at its intersection with the cavity wall or the baffle. Absorption takes place if  $R_\alpha \leq \alpha = \varepsilon$ . If the ray is absorbed, its trajectory ends, and the next ray is traced. On the other hand, if the ray is not absorbed, its point of intersection is determined by constructing a straight-line trajectory based on the random angles  $\theta$  and  $\phi$  of a local spherical coordinate system. At the point of intersection, a second partitioning may take place. Let  $F_{i1}$  denote the view factor of the aperture as seen from the point of impingement

(note that  $F_{i1} = 0$  if the point of intersection is on the baffle). Then, the two partitioned portions are  $F_{i1}(1-F_i)E^*$  and  $(1-F_{i1})(1-F_i)E^*$ . The first of these passes out of the aperture and is tallied. Whereas the second remains in the cavity and continues its life cycle, experiencing successive partitionings until absorption occurs.

Any ray released from a location on the cavity wall will contribute at least one tally (and, perhaps, many tallies) to the determination of the cavity radiant exitance  $E_{\text{out}}$ . The total hemispherical effective emissivity is equal to

$$\varepsilon_e = \frac{E_{\text{out}}}{\sigma T^4 A_a} = \frac{\varepsilon(A_w/A_a)}{N} \left[ \sum_{i=1}^N F_i + \sum_{i=1}^N G_i \right] \quad (95)$$

where  $G_i = 0$ , if no reflections occur;  $G_i = (1-F_i)F_{i1}$  for one reflection;  $G_i = (1-F_i)F_{i1} + (1-F_i)(1-F_{i1})F_{i2}$  for two reflections; and so forth. To avoid a direct hit of the second portions into the aperture, random directions of diffuse emission and reflection were not generated into the entire hemisphere, but into the hemisphere not including the conical solid angle subtended by the aperture. We omit the appropriate trigonometric transformations but note that there is a more simple way: to ignore the traces of the second portion if it hits the aperture, and to generate a new direction.

The cases of emitting and nonemitting baffles were considered. Hemispherical effective emissivities of conical and cylindrical cavities were computed for various values of wall emissivity and geometrical parameters. The convergence of the computational process was studied. Although the energy partitioning method requires time-consuming calculations, the stochastic process converges faster than a conventional Monte Carlo technique. The main drawback of the algorithm described above is its poor applicability to the calculation of the directional effective emissivity, because if a detector of finite size is placed in front of the cavity aperture, the probability of a ray hitting the detector, as well as the view factor for detector, tends to zero as the distance between the aperture and the detector tends to infinity.

#### 4.4.3. Effective emissivity of isothermal specular–diffuse cavities

According to the generalized Kirchhoff's law [11,12] applied to the isothermal opaque cavity:

$$\varepsilon_e = \alpha_e = 1 - \rho_e \quad (96)$$

where  $\varepsilon_e$ ,  $\alpha_e$ , and  $\rho_e$  are the effective emissivity, the effective absorptivity, and the effective reflectivity, respectively.

Consequently, we can consider the reflection of radiation by the cavity, instead of the emission, and replace the conditions of cavity observation with those of cavity irradiation. In this case, rays start at the point of observation,

proceed in the direction of observation, pass through the cavity aperture, and repeatedly reflect off the cavity walls until either they escape the cavity through the aperture or the energy carried by the ray becomes negligible. Such a method is referred to as backward (or inverse) ray tracing. The reversibility of ray trajectories is possible because of the reciprocity principle (see, for instance, Refs. [93,94]) and allows us to evaluate the directional effective emissivity along an infinitely thin ray. Many Monte Carlo algorithms for radiation transfer are based on backward ray tracing.

One such algorithm was developed by Ono in Refs. [95,96] for calculating the directional effective emissivities of isothermal specular–diffuse cavities. He used a serial expression for the directional effective reflectivity of a cylindro–conical cavity:

$$\rho_e^D = \int_A d\Omega_0^1 r_0^{D,1} + \int_W d\Omega_0^1 r_0^{D,1} \int_A d\Omega_1^2 r_1^{0,2} + \dots \tag{97}$$

where  $r_i^j$  is the partial reflectivity (see Section 3.7 and Ref. [57]), and the  $i$ th term  $f_i$  is given by

$$f_i = \int_W d\Omega_0^1 r_0^{D,1} \int_W d\Omega_1^2 r_1^{0,2} \int_W \dots \int_A d\Omega_{i-1}^i r_{i-1}^{i-2,i} \tag{98}$$

Equation (98) expresses  $f_i$  as the fraction of radiation that enters the cavity at the location  $x_0$  from a direction  $D$  and undergoes  $i$  reflections in the cavity according to the partial reflectivity before passing out of the aperture. Thus, the effective reflectivity  $\rho_e^D$  is given by

$$\rho_e^D = \sum_{i=1}^{\infty} f_i \tag{99}$$

For the uniform SD model, reflectance does not depend on the directions of incidence and viewing, so  $r_i^j = r$ . If we set  $r = 1$  (no absorption) in the nested integrals in Equation (97), we can calculate  $\rho_e^D$  for an arbitrary  $r$  by

$$\rho_e^D = \sum_{i=1}^{\infty} F_i r^i \tag{100}$$

where  $F_i$  is the value  $f_i$  in Equation (98) for  $r = 1$ . For a diffuse surface,  $F_1$  is the view factor from the location  $x_0$  to the aperture and  $F_2$  is equivalent to  $I_2$  of Quinn’s formula in Ref. [60], where  $x_0$  is the center of the plane bottom of a diffuse cylindrical cavity.

The standard deviation of the effective reflectivity calculated according to Ono’s method is proportional to  $N^{-1/2}$  such that

$$\Delta\rho \approx \sqrt{\frac{1}{N} \sum_{i=1}^{\infty} F_i r^{2i}} \tag{101}$$

Ono in Refs. [95,96] investigated the normal effective emissivity of isothermal cylindrical and cylindro-conical cavities with specular–diffuse walls using ray tracing and computing the fractions  $F_i$ . In the Figure 8, the normal effective emissivity of the cylindro-conical cavity with the depth-to-diameter ratio  $L/d = 3$  and  $\rho_s/\rho = 0.3$  are depicted as functions of the apex angle  $\theta$  for various values of wall reflectance  $r$ .

Figure 8 shows that the effective emissivity of a cylindro-conical cavity with specular–diffuse walls depends strongly on the conical bottom apex angle. In fact, the normal effective emissivity of a specular–diffuse cylindro-conical cavity is determined by the number of specular reflections of a ray prior to escape from a cavity. The dependence of the effective emissivity on  $\theta$  becomes smoother as the specular fraction of the reflectance decreases.

The same method was applied by Ono et al. [97] to a cylindrical cavity with a lateral hole. In overviews [6] and [98], Ono described his method in detail. Prokhorov et al. [99] described a different algorithm for the numerical modeling of specular–diffuse cavities. They also used the SD model and introduced the diffusity  $D = \rho_d/\rho$ , which does not depend on

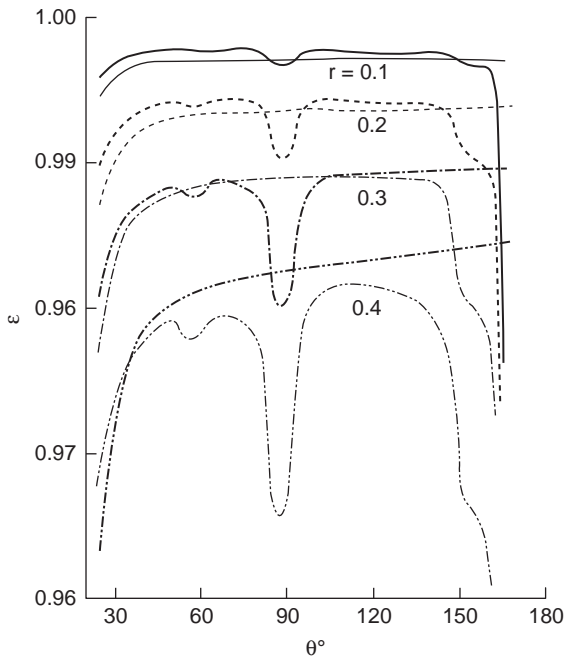


**Figure 8** Normal effective emissivities as a function of the apex angle  $\theta$  of a cylindro-conical cavity with  $L/d = 3$  and  $\rho_s/\rho = 0.3$ , for various surface reflectivities  $r$ . The case of a cavity with a purely diffuse surface is shown by thin lines (from Ref. [95]).

incidence angle. The method of statistical weights was used to accelerate the convergence of the computational process.

The method of statistical weights consists of the following. Before the first interaction with the wall, a statistical weight  $w$  equal to unity is assigned to the ray. After each reflection, the statistical weight is multiplied by the wall reflectance  $\rho$  to obtain a new weight. The effective emissivity is evaluated as the ratio of the sum of the statistical weights of rays escaping the cavity to those launched into the cavity. Ray tracing of a single ray terminates when its statistical weight becomes less than some small, prescribed value, or when the ray leaves the cavity through the aperture after a specular reflection. If the ray hits the aperture after a diffuse reflection, the last direction of reflection is ignored, and a new direction of diffuse reflection is generated.

There exists a strict proof [100] of the fact that the variance of the result obtained by the method of statistical weights is always less than that obtained by the conventional method, which uses the termination of ray trajectories after the absorption event. In the method of statistical weights, each ray, having a statistical weight greater than a predefined threshold value, makes a contribution to the result. The algorithm described in Ref. [99] also includes an analytical calculation of the view factors to the aperture from every point of a diffuse reflection (an analog of the energy partitioning method in Refs. [90–92]).

To save computing time (e.g., when we need to compute the spectral effective emissivity for a large number of wavelengths and the corresponding spectral emissivities of the cavity walls), the method of dependent trials is used. According to it, a set of emissivity values is assigned to the cavity walls, and a corresponding set of statistical weights is assigned to each ray. By transforming the statistical weights at each point of reflection, we use a single trajectory to process a variety of spectral data. This algorithm was applied to the calculation of the effective emissivities of an isothermal specular–diffuse cavity with a conical bottom, a cylindrical middle part, and a tapered conical diaphragm.

Steinfeld [101] used the Monte Carlo method to examine the absorption of a spherical cavity with a specular–diffuse internal surface. If one considers a spherical cavity as a radiation source, then the effective absorptance calculated in this article corresponds to the hemispherical effective emissivity of the source. Chu *et al.* [102] applied the Monte Carlo technique to a cylindrical cavity with an inner-conical bottom and reported good agreement with the results deduced in Ref. [34].

Prokhorov and Hanssen applied backward ray tracing and the method of statistical weights to a cylindrical cavity with a flat diaphragm and a flat inclined bottom [103] (see Figure 9).

It was assumed that the cavity internal walls are uniform and gray. Various conditions of observation were studied. The following estimator

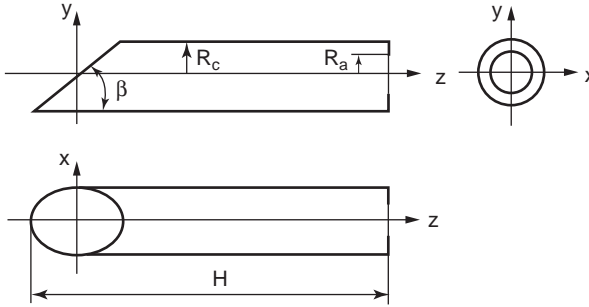


**Figure 9** Cylindrical cavity with an inclined bottom (from Ref. [103]).

for the local directional effective emissivity was obtained:

$$\varepsilon_c(\xi, \omega) = \frac{\varepsilon}{N} \sum_{i=1}^N \sum_{k=1}^{m_i(\xi, \omega)} \rho^{k-1} \quad (102)$$

where  $N$  is the number of rays traced and  $m_i$  the number of reflections of the  $i$ th ray.

The case when the aperture is observed along an infinitely thin ray parallel to the cavity axis corresponds to the local normal effective emissivity. The distribution of the local normal effective emissivity  $\varepsilon_{c,n}(x, y)$  across the aperture is not necessarily uniform.

For a cavity with specular walls, the local normal effective emissivity is

$$\varepsilon_{c,n}(x, y) = 1 - (1 - \varepsilon)^{m(x, y)} \quad (103)$$

where  $m(x, y)$  is the number of successive reflections (prior to escaping the cavity) of a ray that enters into the cavity parallel to the cavity axis and intersects the aperture plane at a point with coordinates  $(x, y)$ .

The  $YZ$  plane is the only plane of symmetry for a cavity with an inclined bottom. When the bottom forms an angle of  $30^\circ$  with the cylinder at  $y = -R_c$  this angle is equal to  $150^\circ$  at  $y = R_c$ . Thus for a purely specular cavity, the rays entering into the cavity aperture through points with coordinates  $(x, y)$  and  $(x, -y)$  after their first reflections from the bottom, fall on the cylindrical wall at different angles. Their further trajectories will also be different, so that the total number of reflections varies.

The points on the aperture that correspond to the same number of reflections form continuous zones of unusual shape. The zones may have irregular structure due to the three-dimensional and nonaxisymmetric nature of the cavity. The shape of these zones can change when  $H$  or  $\beta$  is varied. In Figure 10, a map of the zones of the aperture, which correspond to a certain number of reflections for backward traced rays, is depicted for a specular cavity without a diaphragm,  $R_c = R_a = 1$ ,  $H = 8$ , and  $\beta = 30^\circ$ .

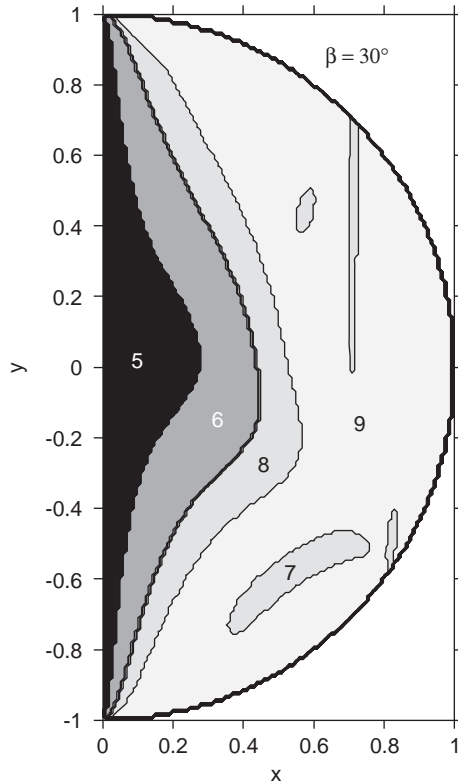


**Figure 10** Distribution of the number of reflections over the aperture of a specular cavity with  $R_c = R_a = 1$ ,  $K = 8$ , and  $\beta = 30^\circ$  (from Ref. [103]).

Numbers on the map indicate the number of reflections for every zone. Because the distribution is symmetrical, only the right half is shown.

Three-dimensional views of the distributions of the local normal effective emissivity  $\varepsilon_{e,n}(x, y)$ , for the cavities with  $R_a = R_c = 1$ ,  $H = 8$ ,  $\beta = 30^\circ$ ,  $\varepsilon = 0.7$ , and  $D = 0, 0.1, 0.5$ , and  $1$  are depicted in Figure 11. For a cavity with purely specular walls, the distribution looks like a set of plateaus, or flat terraces having different heights and often of complicated shape. The presence of a relatively small diffuse component leads to a significant decrease in the distribution's step heights. For instance, at  $D = 0.5$ , the relief created by the distribution of  $\varepsilon_{e,n}(x, y)$  becomes almost indistinct. At  $D = 1$  (purely diffuse walls), the distribution assumes a very smooth convex form with the minimum at  $(x = 0, y = 1)$ .

To compute the average normal effective emissivity  $\varepsilon_{e,n}$ , the same algorithm is used as for the local normal effective emissivity  $\varepsilon_{e,n}(x, y)$ , except that the rays hit the aperture at points that are uniformly distributed over the circular aperture area  $S_a$ .

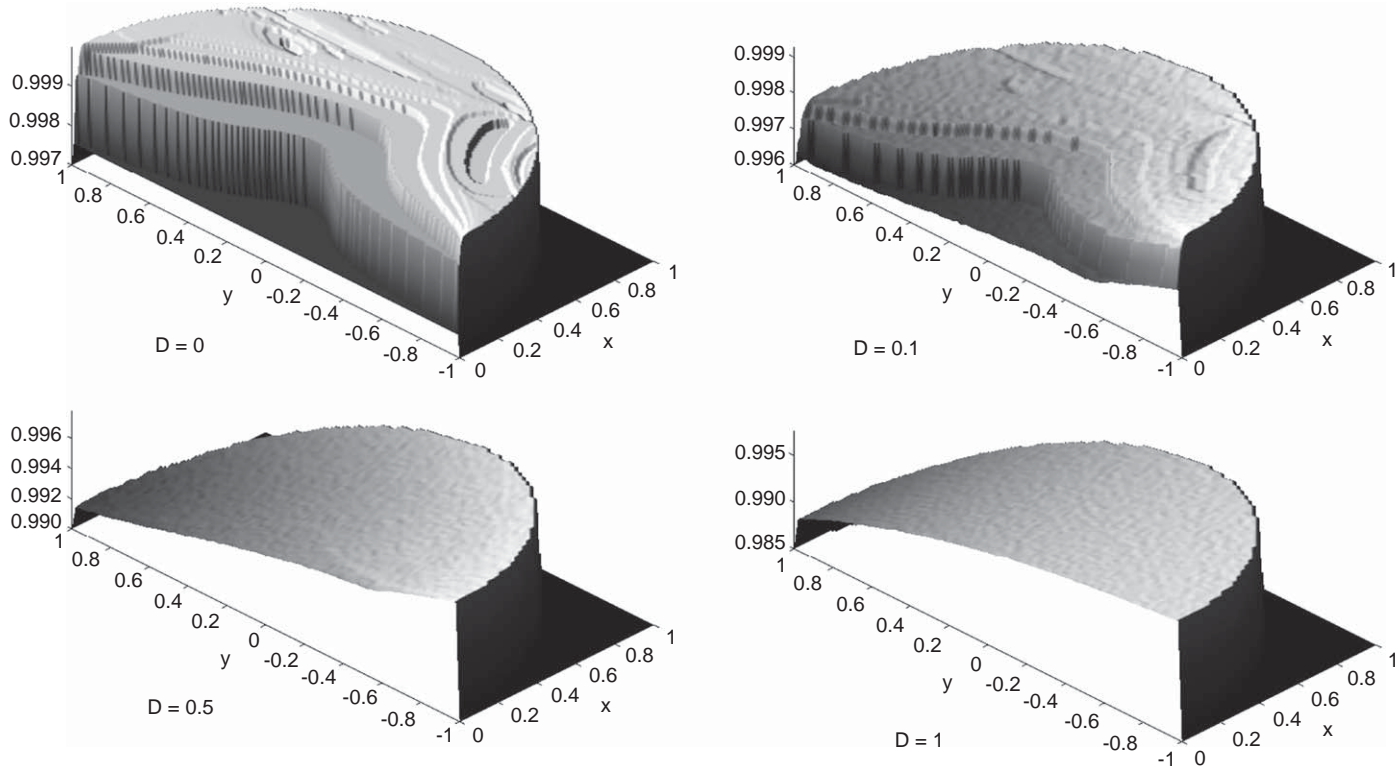


**Figure 11** Distribution of the local normal effective emissivity over the cavity aperture for  $R_a = R_c = 1$ ,  $H = 8$ ,  $\beta = 30^\circ$ ,  $\varepsilon = 0.7$ , and three values of diffusivity,  $D$ . Because of symmetry, only the right halves of the distributions are shown (from Ref. [103]).

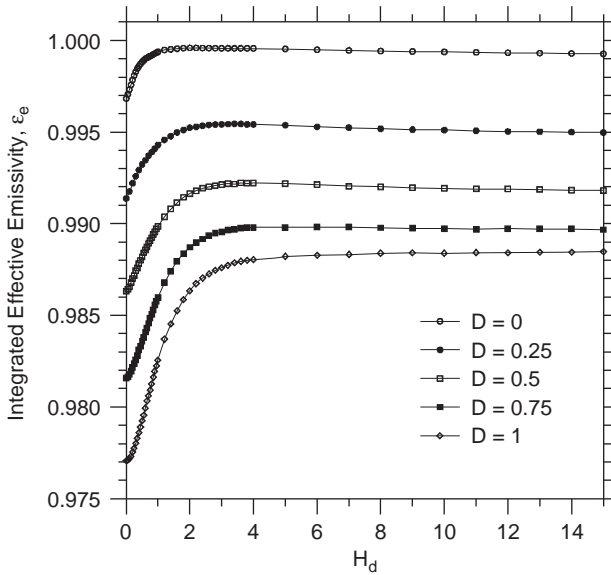


**Figure 12** The integrated effective emissivity of a cavity with a diaphragm as a function of the distance  $H_d$  between the cavity aperture and the detector, for several values of diffusivity,  $D$ ;  $\beta = 30^\circ$ ,  $R_c = 1$ ,  $R_d = R_a = 0.5$ ,  $H = 4$ , and  $\varepsilon = 0.7$  (from Ref. [103]).

The algorithm for calculation of the integrated effective emissivity that allows taking into account the vignetting effect is also described. The integrated effective emissivity of a cavity having  $R_c = 1$ ,  $R_a = 0.5$ ,  $H = 4$ ,  $\beta = 30^\circ$ ,  $\varepsilon = 0.7$ , as a function of the distance  $H_d$  between the cavity aperture and a coaxial circular detector of radius  $R_d$  are plotted in Figure 12 for several values of diffusivity,  $D$ .

Prokhorov et al. [104,105] applied the Monte Carlo method to flat radiators with isothermal concentric grooves of triangular and trapezoidal profiles (Figure 13).

They compared the results obtained for an SD model of reflection using the STEEP3 [106] code, based on the Monte Carlo algorithm [107], with that obtained for Fresnelian–Lambertian (FL) model, whose BRDF is expressed by the equation

$$f_{FL}(\lambda, \theta_i, \phi_i, \theta_r, \phi_r) = d \frac{\rho(\lambda)}{\pi} + (1 - d) F(n_\lambda, k_\lambda, \theta_i) \frac{\delta(\theta_r - \theta_i) \delta(\phi_r - \phi_i \pm \pi)}{\sin \theta_r \cos \theta_i} \tag{104}$$

where the first term is the diffuse (Lambertian) component,  $d$  is the Lambertian BRDF weighting coefficient,  $\delta$  the Dirac’s delta-function,  $\theta_i$  the incidence angle,  $n_\lambda$  the ratio of the spectral refractive indices above and

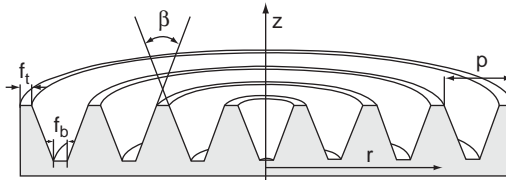


**Figure 13** Geometrical model of the radiator:  $p$  is the pitch,  $f_t$  and  $f_b$  are the widths of the flat areas at the top and bottom, and  $\beta$  is the included angle (from Ref. [104]).

below the surface,  $k_\lambda$  the spectral extinction coefficient, and  $F$  is the Fresnelian reflectance for unpolarized radiation. In general, the following conclusion can be made. Although the FL model is more realistic, it requires sufficient experimental data to fit model parameters. The simpler SD model can be applied when the necessary experimental data are absent. For V-grooved structures, the SD model produces slightly lower values of effective emissivity than the FL model for comparable parameters.

Zhang and Dai [108,109] also used the Monte Carlo ray-tracing technique to calculate the effective emissivity of an infrared blackbody source with a V-grooved bottom, which was assumed to be diffuse and isothermal. Ishii et al. [110] applied a commercially available ray-tracing program, OptiCAD (supplied by OptiCAD Co.) [111] to isothermal cylindro-conical cavities with a grooved cylindrical surface. The SD model of reflection was adopted, following a similar method of calculation as that of Ono [95].

The Monte Carlo method is successfully used for numerical modeling of blackbodies with a reflecting cavity. Quinn and Martin [112] first proposed this blackbody design and Usadi [113] systematically described it. Prokhorov and Martin [114] modeled the radiative heat transfer from such a blackbody of a very sophisticated shape into the cryogenic radiometer. Bidirectional ray tracing was performed with rays propagating first into the radiator and then into the radiometer cavity. Many authors [115–119] have used the Monte Carlo-based software to predict the radiation characteristics of such blackbodies in the design stage.

#### 4.4.4. Effective emissivity of nonisothermal specular–diffuse cavities

The Monte Carlo method has also been applied to the calculation of the radiation characteristics for specular–diffuse cavities that are not isothermal. Sapritsky and Prokhorov [120] proposed a Monte Carlo algorithm to calculate the spectral and total effective emissivity of nonisothermal cavities based on the reciprocity principle and backward ray tracing. The spectral,

local effective emissivity can be written in the form:

$$\varepsilon_c(\lambda, \xi, \omega, T_\xi, T_0) = \varepsilon_c(\lambda, \xi, \omega) + \Delta\varepsilon_c(\lambda, \xi, \omega, T_\xi, T_0) \tag{105}$$

where  $\varepsilon_c(\lambda, \xi, \omega)$  is the local spectral effective emissivity of an isothermal cavity,  $\xi$  and  $\omega$  are the position and direction vectors, respectively, and  $\Delta\varepsilon_c(\lambda, \xi, \omega, T_\xi, T_0)$  is the correction term for nonisothermal conditions.

According to the generalized Kirchhoff's law for isothermal cavities (see Refs. [11,12]):

$$\varepsilon_c(\lambda, \xi, \omega) = 1 - \rho_c(\lambda, \xi, \omega) \tag{106}$$

where  $\rho_c(\lambda, \xi, \omega)$  is the directional-hemispherical spectral effective reflectivity for the direction of radiation incident into the cavity, which coincides with the direction of the observations  $\omega$ . The authors considered the interval  $\lambda_1 \leq \lambda \leq \lambda_2$  where the diffusivity  $D = \rho_d(\lambda)/\rho(\lambda)$  is constant. Initially, each incident ray is assigned a statistical weight of unity, which is multiplied by  $\rho(\lambda)$  following every reflection. Specular or diffuse reflection is selected by means of a pseudorandom number  $u_D$ . If the next pseudorandom number  $u_D < D$ , the reflection is considered to be diffuse. Otherwise, it is specular.

After each diffuse reflection, the statistical weight is reduced to take into account the radiation loss through the cavity aperture. This is done by applying the diffuse view factor  $F_a(\xi)$  between an element of the wall area at the point of reflection  $\xi$  and the cavity aperture. If, after diffuse reflection, a particle escapes from the cavity through the aperture, the last direction of reflection is ignored and the computation begins for another ray. For a fixed number of ray trajectories  $N$ , it is simple to show that

$$\varepsilon_c(\lambda, \xi, \omega) = 1 - \frac{1}{N} \sum_{i=1}^N \sum_{j=1}^{m_i} \rho^j(\lambda) F_a(\xi_j) \prod_{k=1}^{j-1} [1 - F(\xi_k)] \tag{107}$$

where  $m_i$  is the number of reflections in the  $i$ th trajectory. For a specular reflection,  $F_a(\xi) = 1$  if a ray escapes the cavity, otherwise  $F_a(\xi) = 0$ . The maximum number of reflections in the trajectory can be estimated from the relation

$$m = \text{Ent} \left[ \frac{\ln(\delta\varepsilon_{\min})}{\ln(1 - \varepsilon_{\min})} \right] \tag{108}$$

where  $\delta$  is the permissible component of the calculation uncertainty due to the interruption of a ray trajectory,  $\varepsilon_{\min} = \text{Min } \varepsilon(\lambda)$  at  $\lambda_1 \leq \lambda \leq \lambda_2$ .

The spectral directional effective emissivity of a nonisothermal cavity can be calculated using the reciprocity theorem, which permits substitution of the direction of incident radiation into the cavity for the direction of the observation. Each time a ray is reflected from the wall, the spectral radiance of a blackbody is calculated at the cavity wall temperature for that reflection

point in accordance with Planck's law. The weighted summation of these values along the ray trajectory makes it possible to evaluate the spectral radiance at the point  $\xi$  in the direction  $\omega$ . Correction for the nonisothermal case is made using the expression

$$\Delta \varepsilon_c(\lambda, \xi, \omega, T_{\text{ref}}) = \frac{\varepsilon(\lambda)}{NL_c(\lambda, T_{\text{ref}})} \sum_{i=1}^N \sum_{j=1}^{m_i} \rho^{j-1}(\lambda) [L_c(\lambda, T_j) - L_c(\lambda, T_{\text{ref}})] \quad (109)$$

where  $T_j$ ,  $j = 1, 2, \dots, m_i$ , are the cavity wall temperatures at the  $j$ th reflection point.

Sapritsky and Prokhorov in Ref. [121] expanded the applicability of the algorithm [120] and computer code to a cavity having a conical bottom, a conical middle part, and a conical diaphragm. In Ref. [121], the problem of choosing a reference temperature was also discussed. The following hypothesis was suggested: "For each nonisothermal cavity, there is a characteristic reference temperature (called the optimal reference temperature), at which the spectral effective emissivity coincides with that value for the same isothermal cavity." Later, this hypothesis was disproved and in fact we can conclude that such a temperature can be found only as a root-mean-square approximation.

Along with the growth of the performance of personal computers, the algorithm that is described by Equations (107) and (109) has undergone changes. Because cavities with screened walls were included, the algorithm for calculation of the aperture's view factors was eliminated since an increase in the number of rays traced is more effective than the computation of the aperture's view factors. In Ref. [107], the estimator of  $\varepsilon_{\lambda,c}(\lambda, T_{\text{ref}})$  for nonisothermal cavities is

$$\varepsilon_{\lambda,c}(\lambda, T_{\text{ref}}) = \frac{\exp(c_2/(\lambda T_{\text{ref}})) - 1}{N} \sum_{i=1}^N \sum_{j=1}^{m_j} \frac{\varepsilon_j(\lambda)}{\exp(c_2/(\lambda T_j)) - 1} \prod_{k=1}^{j-1} \rho_k(\lambda) \quad (110)$$

Ballico [122] considered the effective emissivity and radiance temperatures of graphite tube blackbody furnace that is observed by a single-wavelength (0.65  $\mu\text{m}$ ) pyrometer with a single-lens objective. From a given element of the blackbody surface, only radiation that (i) lies within the acceptance cone formed by the aperture and source and (ii) passes through the detector image will be detected. Ballico computed the vignetting effect by the zonal method, using the Lambertian approximation and a series of simplifications. If the radiating surface of a cavity is non-Lambertian, the radiance of rays passing through the intersection of the acceptance cone and the detector image varies with the direction. To account for this effect, the Monte Carlo ray-tracing method was applied.

The simple SD model assumes that directional-hemispherical reflectance does not depend on the incidence angle. This assumption is too crude

for the problem considered, so Ballico [122] adopted the FL model. The BRDF can be written as (there is an obvious misprint in Ref. [122], in Equation (21) for BRDF; we provide the corrected formula from Ref. [10] in Ballico's designation):

$$r(\theta_i, \phi_i, \theta_r, \phi_r) = (1 - s) \frac{\rho(\lambda)}{\pi} + sF(\theta_i, \theta_r, n) \frac{\delta(\theta_r - \theta_i) \delta(\phi_r - \phi_i \pm \pi)}{\sin \theta_r \cos \theta_i} \quad (111)$$

where  $s$  is specularity degree and  $\delta$  the Dirac's delta-function,

$$F(\theta_i, \theta_r, n) = \frac{1}{2} \left| \frac{n \cos \theta_i - \cos \chi}{n \cos \theta_i + \cos \chi} \right|^2 + \frac{1}{2} \left| \frac{n \cos \chi - \cos \theta_i}{n \cos \chi + \cos \theta_i} \right|^2 \quad (112)$$

$\sin \chi = (\sin \theta_i)/n$  and  $n$  is the complex refractive index of wall's material.

After ray tracing inside the nonisothermal cavity, the rays are sent through the detection optics, and followed through multiple surface reflections. The solid angle-weighted average of the surface radiances is calculated where the rays are eventually absorbed. The effective emissivity is given by the ratio of the detected power to that received by the pyrometer from the same radiator, but having perfectly black walls. The radiance temperature of a high-temperature graphite tube blackbody was computed through its effective emissivity. The vignetting effect for a pyrometer was also estimated. The Monte Carlo model employed in Ref. [122] has one free parameter, the degree of specularity  $s$  of the surface. A value of  $s$  was fitted using the best agreement between the computed and the measured radiance temperatures as the criterion.

Hartmann and coworkers [123–125] described another Monte Carlo ray-tracing algorithm for computing the spectral effective emissivity of diffuse isothermal and nonisothermal cavities. They also used inverse ray tracing and considered “photons”, which enter the cavity through the aperture. Once the photon reaches the cavity wall, a random number generator is used to determine the next process of the photon. With a probability of  $1 - \varepsilon_w(\lambda)$ , where  $\varepsilon_w(\lambda)$  is the local emissivity of the cavity wall, the photon is reflected from the surface in a randomly distributed direction. The photon is traced until it is either absorbed or reemitted. The effective emissivity  $\varepsilon_{\text{iso}}$  for an isothermal cavity is equal to the ratio of absorbed photons to the photons sent into the cavity. It depends only on the geometry of the cavity and the local emissivity  $\varepsilon_w(\lambda)$  of the cavity walls. For the effective emissivity  $\varepsilon_{\text{noniso}}$  of a nonisothermal cavity, every absorbed photon is weighted by the spectral radiance according to Planck's law at a temperature  $T$  at the location where the photon is absorbed. The spectral radiance  $L(\lambda, T)$  assigned to a single absorbed photon is connected to the spectral radiance  $L_s(\lambda, T)$  of a blackbody at the same temperature by

$$L(\lambda, T) = \varepsilon_w(\lambda) L_s(\lambda, T) \quad (113)$$

For the slightly different temperature  $T - \Delta T$  in a nonisothermal cavity, Equation (113) can be rewritten using Wien's approximation for Planck's law as

$$L(\lambda, T - \Delta T) = \varepsilon_w(\lambda) \left[ 1 - \frac{c_2 \Delta T}{\lambda T^2} \right] L_s(\lambda, T) \tag{114}$$

or, in equivalent form,

$$L(\lambda, T - \Delta T) = \varepsilon_w(\lambda) \varepsilon_{\Delta T, w}(\lambda, \Delta T) L_s(\lambda, T) \tag{115}$$

where  $\varepsilon_{\Delta T, w}(\lambda, \Delta T)$  is the change in local emissivity due to a temperature difference  $\Delta T$ .

Thus, for the entire cavity:

$$L_{\text{cav,iso}} = \frac{1}{N} \sum_n F(\Omega_n) \varepsilon_w(\lambda) L_s(\lambda, T) \tag{116}$$

and

$$L_{\text{cav,noniso}} = \frac{1}{N} \sum_n F(\Omega_n) \varepsilon_w(\lambda) \varepsilon_{\Delta T, w}(\lambda, \Delta T_n) L_s(\lambda, T) \tag{117}$$

The emissivity of a nonisothermal blackbody is

$$\varepsilon_{\text{noniso}} = \frac{1}{N} \sum_n F(\Omega_n) \varepsilon_w(\lambda) \left( 1 - \frac{c_2 \Delta T_n}{\lambda T^2} \right) \tag{118}$$

where  $T$  is the reference temperature (usually, the temperature of the cavity bottom center).

Murthy et al. [126] applied the Monte Carlo method to computer modeling of heat-flux sensor calibration using a high-temperature blackbody and the cooled sensor placed inside the blackbody to achieve higher heat-flux levels in a nearly hemispherical irradiation environment. The blackbody radiator and an inserted heat-flux sensor differ widely in temperature. In addition, the sensor's surface partially reflects the radiation falling on it. The computations make possible the determination of the optimum distance from the sensor to the cavity bottom in order to attain the maximal value of the effective emissivity and hence the maximal radiative heat flux.

Ishii et al. [127] performed ray tracing of blackbody cavities that serve as the standard sources for calibration of infrared ear thermometers. Including the effect of the background radiation, they obtained the following expression for the spectral effective emissivity:

$$\varepsilon_e(\lambda) = \frac{1}{N} \sum_{n=1}^N \left[ \sum_{k=1}^{k_n} \alpha(\lambda) \rho^{k-1}(\lambda) R_{\lambda, b}(\lambda, T(n, k), T_0) + \rho^{k_n}(\lambda) R_{\lambda, b}(\lambda, T_s, T_0) \right] \tag{119}$$

where  $\alpha(\lambda)$  is the directional absorptance and  $\rho(\lambda)$  the directional-hemispherical reflectance of the surface given by  $\rho(\lambda) = 1 - \alpha(\lambda)$  for an opaque body.  $N$  is the total number of incident ray bundles,  $k_n$  the total number of reflections of the  $n$ th ray bundle inside the cavity,  $T(n, k)$  the temperature at the location  $x(n, k)$ , for which an  $n$ th ray bundle reaches the cavity inner surface at the  $k$ th impact,  $R_{\lambda,b}(\lambda, T(n, k), T_0)$  the blackbody spectral radiance ratio at the wavelength  $\lambda$  between the local temperature  $T(n, k)$  and the reference temperature  $T_0$  and  $T_s$  is the temperature of the surroundings. The angular dependence of the effective emissivity of nonisothermal cavities, with the shape of cylindro-cone and a cylinder with an inclined bottom, which are suitable for the calibration of ear thermometers with wide view angles, was investigated.

#### 4.5. Modeling of direction-dependent optical characteristics

The SD model of reflection is sufficiently powerful to calculate the effective emissivity of blackbody cavities in most practical cases. However, for some situations and materials, the SD model cannot ensure the precision necessary to satisfy modern metrological requirements. One of the major advantages of the Monte Carlo method is the possibility to model optical radiation transfer between surfaces with directionally dependent optical characteristics, including random rough surfaces.

To model optical radiation transfer between non-Lambertian surfaces using the Monte Carlo method, it is necessary to generate random directions of reflection using a distribution of the probability density that is determined by the BRDF of the reflecting surface. Since measurements of BRDF are usually carried out for a limited range of angles of incidence and reflection, it is necessary to have a model of BRDF that reproduces the measurement results with sufficient accuracy, has physically plausible behavior within the entire domain of its definition, and has a directional-hemispherical reflectance that depends on the incident angle in accordance with experimental data.

Zaworski et al. [128] computed the spatial distribution of radiation passed through a rectangular gap with rough walls. The polar and azimuthal spherical coordinates for the reflection lobe were considered as Gaussian variates with respect to the specular direction. Standard deviations of Gaussian distributions were fitted to experimental data. However, a significant discrepancy between the computed and measured resulting distributions of radiation passed through the gap was obtained. The authors suggested that the discrepancy is due to a lack of measured values of the bidirectional reflectance at large incident angles and deficiencies of the model adopted.

A better approach to modeling a random rough surface must have a physical basis. Micro-facet based models represent a rough surface as a

collection of planar mirror-like facets randomly tilted with respect to the plane of the horizon. The size of the micro-facets must be small enough as compared to an irradiated area for statistics methods to be applicable. Torrance and Sparrow [129] proposed a one-dimensional micro-facet model of a rough surface consisting of randomly oriented equilateral V-grooves with random Gaussian slopes. Only the first reflection is considered and the analytical expression is derived for a geometric attenuation factor, allowing for masking and shadowing effects (partial illumination of a facet shadowed by an adjacent one and the partial visibility of a facet occluded by another). Although this model is very simple, it predicts the peak shift in the BRDF at large incidence angles toward larger reflection angles. These off-specular peaks are observable experimentally for all rough materials. The Torrance–Sparrow model does have an intrinsic defect: its directional-hemispherical reflectance depends on incidence angle even when the facet’s reflectance is equal to unity. However, because of its simplicity, the use of the Torrance–Sparrow model continues to spread in the fields of computer graphics, remote sensing, and radiation heat transfer.

Zhou et al. [130] applied a modified Ward’s model of reflection [131] to Monte Carlo modeling of the effective emissivity of a rough silicon wafer. Further modifications to the model may be necessary to obtain better agreement of the incidence angle dependence of the directional-hemispherical reflectance with experimental data.

Prokhorov et al. [132] and Hanssen and Prokhorov [133] described a new model of reflection from rough surfaces, referred to as the TETRA BRDF model that is also based on micro-facet theory and developed within the framework of geometric optics. It employs the generation of random tetrahedral pits (see Figure 14), whose walls reflect each ray according to Fresnel’s law. Several arrangement types for the projection of the lower tetrahedron vertex onto the tangent plane were considered: (R) a random point uniformly distributed inside the base triangle, (G) the base triangle centroid (center of gravity), (V) one of the vertices of the base triangle, and (C) the circumcircle center.

The depth  $h$  of the tetrahedral pit is considered as a random variate distributed according to the two-parameter Weibull probability density defined as

$$p(h) = \frac{\beta}{\eta^\beta} h^{\beta-1} \exp \left[ - \left( \frac{h}{\eta} \right)^\beta \right], \quad h > 0 \quad (120)$$

where  $\beta > 0$  is the shape parameter and  $\eta > 0$  is the scale parameter of the distribution.

An incident ray undergoes one or several reflections from the tetrahedron’s walls, and then continues to participate in the radiation transfer on the macro-level. If a large number of rays are aimed at the same

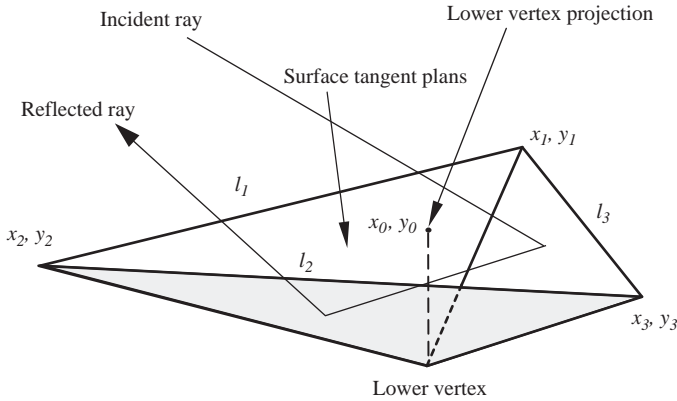


**Figure 14** Tetrahedral pit with a triangular base in the surface tangent plane (from Ref. [132]).

point of a surface along the same direction and the rays scattered by the random tetrahedrons are registered, one can construct a resultant BRDF.

This procedural model of reflection has as a prototype the two-dimensional model proposed by Torrance and Sparrow. The in-plane sections of the TETRA-G, TETRA-V, TETRA-R, and TETRA-C BRDFs generated for  $\beta = 2$ ,  $\eta = 0.1$ , and incident angles of  $0^\circ$ ,  $30^\circ$ , and  $60^\circ$  are shown in Figure 15. Three-dimensional plots of the TETRA-G BRDF in spherical coordinates for  $\beta = 2$ ,  $n_\lambda = 2.5$ ,  $k_\lambda = 2.0$ , and  $\lambda = 10.6 \mu\text{m}$  and for three incidence angles are presented in Figure 16, where all BRDF maxima are normalized to unity.

The local directional spectral effective emissivity of a cavity having an arbitrary temperature distribution over a radiating surface can be computed by the following equation:

$$\varepsilon_c(\lambda, T_{\text{ref}}, \xi_0, \omega_0) = \frac{1 - \rho(\lambda, \xi_0, \omega_0)}{NL_{\lambda, \text{bb}}(\lambda, T_{\text{ref}})} \sum_{i=1}^N \sum_{j=1}^{m_i} L_{\lambda, \text{bb}}(\lambda, T_{ij}) \prod_{k=0}^{j-1} \rho(\lambda, \xi_{ik}, \omega_{ik}) \quad (121)$$

where  $\omega_k$  is the direction of the incidence of the  $i$ th ray onto the  $k$ th point,  $\xi_k$  of reflection;  $\xi_0$  and  $\omega_0$  are the viewing point and the viewing direction, respectively,  $\rho$  is the directional-hemispherical reflectance, and  $T_{ij}$  the temperature at the point of the  $j$ th reflection of the  $i$ th trajectory.

As an example, the distributions of the local normal effective emissivity across the aperture were computed for a conical cavity with an apex angle  $\beta = 30^\circ$ , without a diaphragm and a cylindrical cavity with a diaphragm, and with a radius of the bottom  $R_c = 1$ , an aperture radius  $R_a = 0.5$ , and a length  $L = 4$ . Both cavities are assumed to be isothermal. The results of the calculations are presented in Figures 17 and 18. It was assumed that the

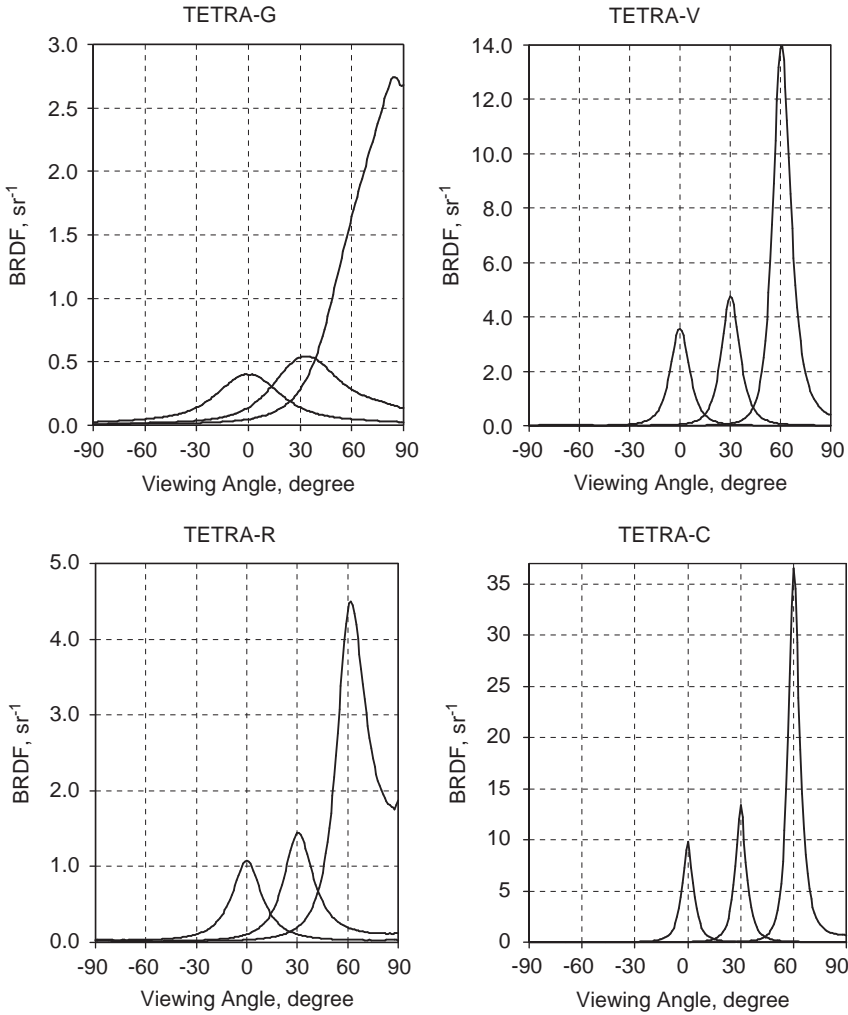


**Figure 15** In-plane TETRA-G, TETRA-V, TETRA-R, and TETRA-C BRDFs generated for  $\beta = 2$ ,  $\eta = 0.1$ , and incident angles of  $0^\circ$ ,  $30^\circ$ , and  $60^\circ$  (from Ref. [132]).

reflection from a tetrahedron's facet obeys Fresnel's law and that  $n_\lambda = 2.5$  and  $k_\lambda = 2.0$ .

For comparison, calculations were also performed for various diffusivities  $D$  within the framework of the conventional SD model, in which the reflectance  $\rho$  was chosen to be numerically equal to the Fresnelian reflectance for normal incidence. For each surface, the directional-hemispherical reflectance for a set of incident angles is computed prior to ray tracing, then, during ray tracing, interpolation is used.

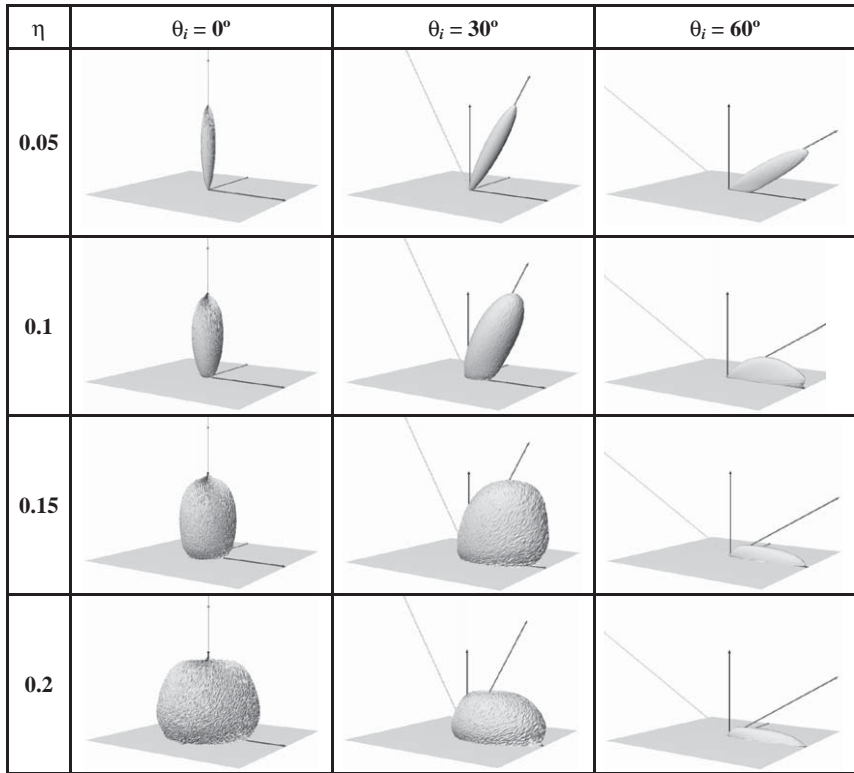


**Figure 16** 3D plots of the TETRA-G BRDF in spherical coordinates for three incident angles;  $\beta = 2$ ,  $n_\lambda = 2.5$ ,  $k_\lambda = 2.0$ , and  $\lambda = 10.6 \mu\text{m}$ . All BRDF maxima are normalized to unity (from Ref. [132]).

Figures 17 and 18 show significant differences in the distributions obtained for the two models. None of the dependences computed for the TETRA model can be approximated by the dependences computed for the specular–diffuse one. In addition, the calculations performed for a cylindrical cavity (Figure 18) using the TETRA model predict a significantly greater nonuniformity of the distribution of normal effective emissivity over the cavity aperture than that for the SD model.



## 5. NUMERICAL COMPARISON OF RESULTS OBTAINED BY VARIOUS METHODS

Several computational techniques of the effective emissivity are in current use. McEvoy et al. [134] compared calculations of the effective emissivity performed with the help of several programs. The first was a

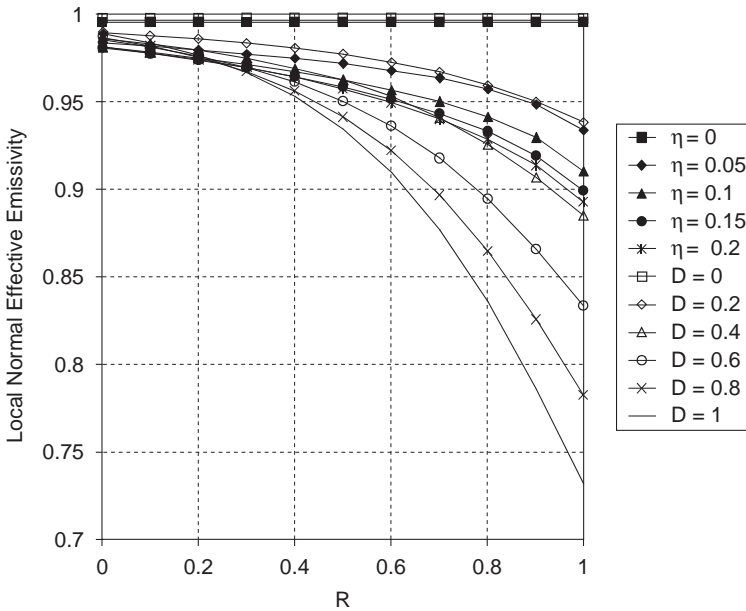


**Figure 17** Distributions of the local normal effective emissivity across the aperture of an isothermal conical cavity with an apex angle of  $30^\circ$  computed for the TETRA and specular–diffuse models of reflection plane (from Ref. [132]).

program written at the National Physical Laboratory (UK) [63] to calculate the emissivity of an isothermal cylindrical cavity with a reentrant cone on the back wall by de Vos's method [57]. A correction term for nonisothermal conditions was also calculated. The emissivity was also calculated using a different program, the commercially available, modeling program, STEEP3 [106]. For a graphite wall with an emissivity  $\varepsilon = 0.92$ , both programs gave an estimate for the total emissivity of the cavity, of 0.99998. This corresponds to a temperature correction at the Ag melting point of 2 mK at  $\lambda = 906$  nm. To assess the dependence of the cavity emissivity on the value chosen for the wall emissivity, the calculation was repeated for graphite walls with an emissivity of 0.81. In this case, the estimated emissivity of the cavity was 0.99996, a temperature correction at the Ag melting point of 4 mK at  $\lambda = 906$  nm.

To provide further verification of the validity of the software, the emissivity of the cavity was calculated at the Physikalisch-Technische Bundesanstalt (Germany) using their emissivity software [123–125]. It calculates emissivities of isothermal and nonisothermal cavities based on a Monte Carlo ray-tracing method. Assuming an isothermal cavity with wall emissivities of 0.92 and 0.81 the cavity emissivities were found to be 0.99999 and 0.99997, respectively. The results from all three programs

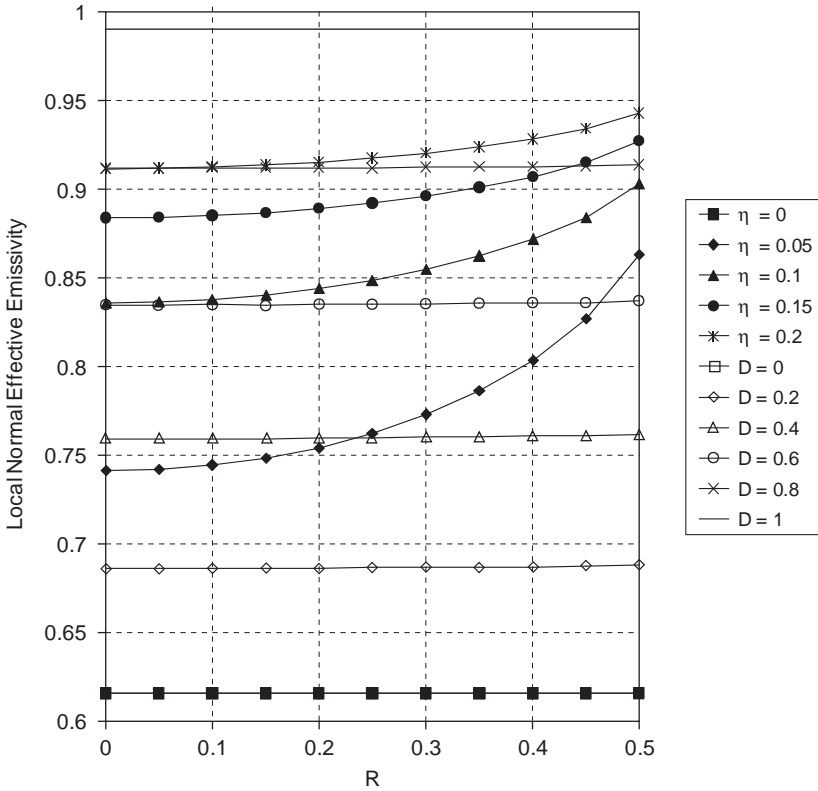


**Figure 18** Distributions of the local normal effective emissivity across the aperture of an isothermal cylindrical cavity with  $R_c = 1$ ,  $R_a = 0.5$ , and  $H = 4$  computed for the TETRA and specular–diffuse models of the reflection (from Ref. [132]).

agreed to within  $1 \times 10^{-5}$  (which corresponds to the difference in radiance temperature of 1 mK at 950 nm and 0.7 mK at 650 nm), providing confidence in the validity of the software.

The time has perhaps arrived to conduct a more comprehensive intercomparison of various software tools being used for the calculation of effective emissivity with an aim to deduce their actual accuracy. Clearly, the experimental verification must remain the *ultima ratio* in determining a preference of one computational method over another.

## 6. CONCLUSIONS

Calibration of radiation thermometers is performed using blackbody radiation sources. Radiation thermometry metrology is impossible without

a reliable determination of the radiation characteristics of such sources. Of primary importance is the effective emissivity. In most instances, calculation is the only way to determine the effective emissivity. In order to achieve the necessary accuracy, even the most advanced computational method must be based on experimental data of temperature and optical properties of the cavity's walls.

In this chapter, we have considered both conventional (deterministic) and stochastic (Monte Carlo ray tracing) methods for the effective emissivity computational determination and made an attempt to show the advantages of the stochastic methods. However, this is not to say that the deterministic, especially, analytic (i.e., formula-based) methods must be excluded from consideration. They allow investigation of the most general dependences and trends, despite their limited accuracy or applicability.

Issues such as the numerical modeling of the temperature distributions over a cavity's radiating surface, polarization of the radiation emitted by a blackbody cavity (which can be important especially for cavities whose walls have a significant specular reflection), the scattering and refraction of a cavity's radiation, etc., remain beyond the scope of this chapter and require additional discussion.

## ACKNOWLEDGEMENT

The authors wish to acknowledge the considerable effort of Catherine Cooksey in helping to edit this Chapter and thereby making the content more accessible to its readers.

## REFERENCES

- [1] E. M. Sparrow and R. D. Cess, *Radiation Heat Transfer*, Hemisphere, Washington, DC (1978).
- [2] R. Siegel and J. Howell, *Thermal Radiation Heat Transfer*, Taylor & Francis, New York, 4th ed. (2002).
- [3] M. F. Modest, *Radiative Heat Transfer*, Academic Press, New York, 2nd ed. (2003).
- [4] H. C. Hottel and A. F. Sarofim, *Radiative Transfer*, McGraw-Hill, New York (1967).
- [5] R. E. Bedford, "Calculation of Effective Emissivities of Cavity Sources of Thermal Radiation," in *Theory and Practice of Radiation Thermometry*, edited by D. P. DeWitt and G. D. Nutter, Wiley, New York, pp. 653–772 (1988).
- [6] A. Ono, "Methods for Reducing Emissivity Effects," in *Theory and Practice of Radiation Thermometry*, edited by D. P. DeWitt and G. D. Nutter, Wiley, New York, pp. 565–624 (1988).
- [7] R. E. Bedford, "Effective Emissivities of Blackbody Cavities – A Review," in *Temperature: Its Measurement and Control in Science and Industry*, edited by H. H. Plumb, Instrument Society of America, Pittsburgh, PA, Vol. 4, Part 1, pp. 425–434 (1972).
- [8] T. J. Quinn, *Temperature*, Academic Press, London, 2nd ed. (1990).

- [9] P. J. Mohr, B. N. Taylor, and D. B. Newell, "The Fundamental Physical Constants," *Phys. Today* **60**, 55 (2007).
- [10] F. E. Nicodemus, J. C. Richmond, J. J. Hsia, I. W. Ginsberg, and T. Limperis, *Geometrical Considerations and Nomenclature for Reflectance*, NBS Monograph 160, US Department of Commerce, National Bureau of Standards (1977).
- [11] F. J. Kelly, "On Kirchhoff's Law and Its Generalized Application to Absorption and Emission by Cavities," *J. Res. Natl. Bur. Stand. – B. Math. Math. Phys.* **69B**, 165–171 (1965).
- [12] Y. Ohwada, "Mathematical Proof of an Extended Kirchhoff Law for a Cavity Having Direction-Dependent Characteristics," *J. Opt. Soc. Am. A* **5**, 141–145 (1988).
- [13] G. Ribaud, *Traité de Pyrométrie Optique*, Revue d'Optique, Paris (1931).
- [14] A. Gouffé, "Correction d'ouverture des corps-noirs artificiels compte tenu des diffusions multiples internes," *Revue d'Optique Théorique et Instrumentale* **24**, 1–10 (1945).
- [15] E. W. Treuenfels, "Emissivity of Isothermal Cavities," *J. Opt. Soc. Am.* **53**, 1162–1171 (1963).
- [16] K. G. T. Hollands, *Thermal Radiation Fundamentals*, Begell House, New York (2004).
- [17] A. D. Polyanin and A. V. Manzhirov, *Handbook of Integral Equations*, Chapman & Hall/CRC, Boca Raton, FL, 2nd ed. (2008).
- [18] P. Kythe and P. Puri, *Computational Methods for Linear Integral Equations*, Birkhäuser, Boston, MA (2002).
- [19] K. E. Atkinson, *The Numerical Solution of Integral Equations of the Second Kind*, Cambridge University Press, Cambridge (1997).
- [20] E. M. Sparrow, "Radiant Absorption Characteristics of Concave Cylindrical Surfaces," *J. Heat Transfer* **84**, 283–293 (1962).
- [21] E. M. Sparrow and V. K. Jonsson, "Absorption and Emission Characteristics of Diffuse Spherical Enclosures," *J. Heat Transfer* **84**, 188–189 (1962).
- [22] M. J. Caola, "Radiation from a Nonisothermal Spherical Cavity: An Exact Solution," *Appl. Opt.* **40**, 3232–3234 (2001).
- [23] Y. Ohwada, "Formulation of Multiple Reflections within a Diffuse Cavity Radiator: Comments," *Appl. Opt.* **23**, 4181–4182 (1984).
- [24] C. L. Sydnor, "Series Representation of the Solution of the Integral Equation for Emissivity of Cavities," *J. Opt. Soc. Am.* **59**, 1288–1290 (1969).
- [25] W. H. Press, S. A. Teukolsky, W. T. Vetterling, and B. P. Flannery, *Numerical Recipes. The Art of Scientific Computing*, Cambridge University Press, Cambridge, 3rd ed. (2007).
- [26] E. M. Sparrow, L. U. Albers, and E. R. G. Eckert, "Thermal Radiation Characteristics of Cylindrical Enclosures," *J. Heat Transfer* **84**, 73–81 (1962).
- [27] E. M. Sparrow and V. K. Jonsson, "Radiant Emission Characteristics of Diffuse Conical Cavities," *J. Opt. Soc. Am.* **53**, 816–821 (1963).
- [28] G. Alfano, "Emissione Termica di Cavità Cilindriche Parzialmente Chiuse da Diaframmi," *La Termotecnica* **24**, 215–223 (1970).
- [29] G. Alfano, "Apparent Thermal Emittance of Cylindrical Enclosures with and without Diaphragms," *Int. J. Heat Mass Transfer* **15**, 2671–2674 (1971).
- [30] F. J. Kelly, "An Equation for the Local Thermal Emissivity at the Vertex of a Diffuse Conical or V-Groove Cavity," *Appl. Opt.* **5**, 925–927 (1966).
- [31] R. E. Bedford and C. K. Ma, "Emissivities of Diffuse Cavities: Isothermal and Nonisothermal Cones and Cylinders," *J. Opt. Soc. Am.* **64**, 339–349 (1974).
- [32] R. E. Bedford and C. K. Ma, "Emissivities of Diffuse Cavities, II: Isothermal and Nonisothermal Cylindro-Cones," *J. Opt. Soc. Am.* **65**, 565–572 (1975).
- [33] R. E. Bedford and C. K. Ma, "Emissivities of Diffuse Cavities, III: Isothermal and Nonisothermal Double Cones," *J. Opt. Soc. Am.* **66**, 724–730 (1976).

- [34] R. E. Bedford, C. K. Ma, Z. Chu, Y. Sun, and S. Chen, "Emissivities of Diffuse Cavities. 4: Isothermal and Nonisothermal Cyllindro-Inner-Cones," *Appl. Opt.* **24**, 2971–2980 (1985).
- [35] H. Yamamoto, "Precise Evaluation of the Effective Emissivity of Cavity Radiators," *Bull. NRLM* **22**, 4–9 (1971).
- [36] R. J. Chandos and R. E. Chandos, "Radiometric Properties of Isothermal, Diffuse Wall Cavity Sources," *Appl. Opt.* **13**, 2142–2152 (1974).
- [37] K. E. Atkinson, "The Numerical Solution of Fredholm Integral Equations of the Second Kind," *SIAM J. Numer. Anal.* **4**, 337–348 (1967).
- [38] S. R. Meier, R. I. Joseph, and S. K. Antiochos, "Radiation Characteristics of a High-Emissivity Cylindrical–Spherical Cavity with Obscuration," *J. Opt. Soc. Am. A* **21**, 104–112 (2004).
- [39] E. M. Sparrow and R. P. Heinisch, "The Normal Emittance of Circular Cylindrical Cavities," *Appl. Opt.* **9**, 2569–2572 (1970).
- [40] G. Alfano and A. Samö, "Normal and Hemispherical Thermal Emittances of Cylindrical Cavities," *J. Heat Transfer* **97**, 387–390 (1975).
- [41] S. Chen, Z. Chu, and H. Chen, "Precise Calculation of the Integrated Emissivity of Baffled Blackbody Cavities," *Metrologia* **16**, 69–72 (1980).
- [42] Z. Chu, R. E. Bedford, W. Xu, and X. Liu, "General Formulation for the Integrated Effective Emissivity of Any Axisymmetric Diffuse Blackbody Cavity," *Appl. Opt.* **28**, 1826–1829 (1989).
- [43] Z. Chu, J. He, J. Dai, W. Chen, and R. E. Bedford, "Formulation for the Integrated Effective Emissivity of Any Diffuse, Circularly-Symmetric Blackbody Cavity," *High Temp.-High Pressures* **25**, 607–612 (1993).
- [44] Y. Ohwada, "Numerical Calculation of the Effective Emissivities of Diffuse Cones with a Series Technique," *Appl. Opt.* **20**, 3332–3335 (1981).
- [45] Y. Ohwada, "Numerical Calculation of the Effective Emissivity by Using a Series Technique," in *Temperature: Its Measurement and Control in Science and Industry*, edited by J. F. Schooley, American Institute of Physics, Vol. 5, pp. 517–519 (1982).
- [46] Y. Ohwada, "Numerical Calculation of Multiple Reflections in Diffuse Cavities," *J. Opt. Soc. Am.* **71**, 106–111 (1981).
- [47] Y. Ohwada, "Evaluation of Integrated Emissivity of a Black Body," *Jpn. J. Appl. Phys., Part 2 (Lett.)* **23**, 167–168 (1984).
- [48] Y. Ohwada, "Evaluation of Effective Emissivities of Nonisothermal Cavities," *Appl. Opt.* **22**, 2322–2325 (1983).
- [49] Y. Ohwada, "Numerical Calculation of Bandlimited Effective Emissivity," *Appl. Opt.* **24**, 280–283 (1985).
- [50] Y. Ohwada and H. Sakate, "Effective Emissivity of an Isothermal Cylinder Having a Longitudinal Strip Opening," *Appl. Opt.* **26**, 3186–3187 (1987).
- [51] Y. Ohwada, "Influence of Deviation from Lambertian Reflectance on the Effective Emissivity of a Cavity," *Metrologia* **32**, 713–716 (1995).
- [52] Y. Ohwada, "Calculation of the Effective Emissivity of a Cavity Having non-Lambertian Isothermal Surfaces," *J. Opt. Soc. Am. A* **16**, 1056–1065 (1999).
- [53] T. J. Quinn, "The Absorptivity of a Specularly Reflecting Cone for Oblique Angles of View," *Infrared Phys.* **21**, 123–126 (1981).
- [54] Z. Chu, Y. Sun, R. E. Bedford, and C. K. Ma, "Precise Calculation of Effective Emissivity of a Diffuse Cyllindro-Inner-Cone with a Specular Lid," *Appl. Opt.* **25**, 4343–4348 (1986).
- [55] S. H. Lin and E. M. Sparrow, "Radiant Interchange among Curved Specularly Reflecting Surfaces – Application to Cylindrical and Conical Cavities," *J. Heat Transfer* **88**, 299–307 (1965).

- [56] F. Kowsary and J. R. Mahan, "Radiative Characteristic of Spherical Cavities with Specular Reflectivity Component," *J. Heat Transfer* **128**, 261–268 (2006).
- [57] J. C. De Vos, "Evaluation of the Quality of a Blackbody," *Physica (Utrecht)* **20**, 669–689 (1954).
- [58] P. Campanaro and T. Ricolfi, "Effective Emissivity of a Spherical Cavity," *Appl. Opt.* **5**, 929–932 (1966).
- [59] P. Campanaro and T. Ricolfi, "Radiant Emission Characteristics of a Nonisothermal Spherical Cavity," *Appl. Opt.* **5**, 1271–1273 (1966).
- [60] T. J. Quinn, "The Calculation of the Emissivity of Cylindrical Cavities Giving near Black-Body Radiation," *Br. J. Appl. Phys.* **18**, 1105–1113 (1967).
- [61] T. J. Quinn and J. E. Martin, "A Radiometric Determination of the Stefan–Boltzmann Constant and Thermodynamic Temperatures between –40 Degrees C and +100 Degrees C," *Philos. Trans. R. Soc. Lond., Ser. A, Math. Phys. Sci.* **316**, 85–189 (1985).
- [62] K. H. Berry, "Emissivity of a Cylindrical Black-Body Cavity with a Re-entrant Cone end Face," *J. Phys. E: Sci. Instrum.* **14**, 629–632 (1981).
- [63] J. S. Redgrove and K. H. Berry, "Emissivity of a Cylindrical Blackbody Cavity Having Diffuse and Specular Components of Reflectivity with a Correction Term for Nonisothermal Conditions," *High Temp.-High Pressures* **15**, 1–11 (1983).
- [64] J. S. Liu, *Monte Carlo Strategies in Scientific Computing*, Springer, New York, 2nd ed. (2008).
- [65] G. S. Fishman, *Monte Carlo. Concepts, Algorithms, and Applications*, Springer, New York (1995).
- [66] I. Manno, *Introduction to the Monte Carlo Method*, Akadémiai Kiadó, Budapest (1999).
- [67] R. Y. Rubinstein and D. P. Kroese, *Simulation and the Monte Carlo Method*, Wiley, New York (2007).
- [68] I. T. Dimov, *Monte Carlo Methods for Applied Scientists*, World Scientific, London, (2008).
- [69] M. H. Kalos and P. A. Whitlock, *Monte Carlo Methods*, Wiley, New York (1986).
- [70] N. Metropolis and S. Ulam, "The Monte Carlo Method," *J. Am. Stat. Assoc.* **44**, 335–341 (1949).
- [71] G. I. Marchuk, *Monte Carlo Methods in Atmospheric Optics*, Springer, New York (1980).
- [72] J. R. Mahan, *Radiation Heat Transfer: A Statistical Approach*, Wiley, New York (2002).
- [73] J. R. Howell, "The Monte Carlo Method in Radiative Heat Transfer," *J. Heat Transfer* **120**, 547–560 (1998).
- [74] P. Shirley, M. Ashikhmin, M. Gleicher, and S. Marschner, *Fundamentals of Computer Graphics*, A K Peters, Natick, MA, 2nd ed. (2005).
- [75] P. Shirley and R. K. Morley, *Realistic Ray Tracing*, A K Peters, Natick, MA, 2nd ed. (2003).
- [76] H. W. Jensen, *Realistic Image Synthesis Using Photon Mapping*, A K Peters, Natick, MA (2001).
- [77] A. S. Glassner (ed.), *An Introduction to Ray Tracing*, Morgan Kaufmann, San Francisco, CA (1989).
- [78] J. T. Gentle, *Random Number Generation and Monte Carlo Methods*, Springer, New York, 2nd ed. (2004).
- [79] P. L'Ecuyer, "Uniform Random Number Generators," in *Proceedings of the Winter Simulation Conference*, ACM, Washington, DC, pp. 97–104 (1998).
- [80] K. Entacher, "Bad Subsequences of Well-Known Linear Congruential Pseudorandom Number Generators," *ACM Trans. Model. Comput. Simul.* **8**, 61–70 (1998).

- [81] A. V. Prokhorov, S. N. Mekhontsev, and L. M. Hanssen, "Monte Carlo Modeling of an Integrating Sphere Reflectometer," *Appl. Opt.* **42**, 3832–3842 (2003).
- [82] M. Matsumoto and T. Nishimura, "Mersenne Twister: A 623-Dimensionally Equidistributed Uniform Pseudo-Random Number Generator," *ACM Trans. Model. Comput. Simul.* **8**, 3–30 (1998).
- [83] "Mersenne Twister Home Page," <http://www.math.sci.hiroshima-u.ac.jp/~m-mat/MT/emt.html> (2008).
- [84] G. Glaeser, *Fast Algorithms for 3D-Graphics*, Springer, New York (1993).
- [85] R. Srinivasan, *Importance Sampling – Applications in Communications and Detection*, Springer, Berlin (2002).
- [86] L. G. Polgar and J. R. Howell, *Directional Thermal-Radiative Properties of Conical Cavities*, NASA TN D-2904 (1965).
- [87] R. C. Corlett, "Direct Numerical Simulation of Thermal Radiation in Vacuum," *ASME J. Heat Transfer* **88**, 376–382 (1966).
- [88] J. S. Toor and R. A. Viskanta, "Numerical Experiment of Radiant Heat Interchange by the Monte Carlo Method," *Int. J. Heat Mass Transfer* **11**, 883–897 (1968).
- [89] P. Beckmann and A. Spizzichino, *The Scattering of Electromagnetic Waves from Rough Surface*, Macmillan, New York (1963).
- [90] R. P. Heinisch, E. M. Sparrow, and N. Shamsundar, "Radiant Emission from Baffled Conical Cavities," *J. Opt. Soc. Am.* **63**, 152–158 (1973).
- [91] N. Shamsundar, E. M. Sparrow, and R. P. Heinisch, "Monte Carlo Radiation Solutions – Effect of Energy Partitioning and Number of Rays," *Int. J. Heat Mass Transfer* **16**, 690–694 (1973).
- [92] E. M. Sparrow, R. P. Heinisch, and N. Shamsundar, "Apparent Hemispherical Emittance of Baffled Cylindrical Cavities," *J. Heat Transfer* **96**, 112–114 (1974).
- [93] W. C. Snyder, "Reciprocity of the Bidirectional Reflectance Distribution Function (BRDF) in Measurements and Models of Structured Surfaces," *IEEE Trans. Geosci. Remote Sens.* **36**, 685–691 (1998).
- [94] A. Prokhorov, S. Mekhontsev, and L. Hanssen, "Reciprocity Principle and Choice of the Reflectance Model for Physically Correct Modeling of Effective Emissivity," in *Temperature: Its Measurement and Control in Science and Industry*, edited by D. C. Ripple, American Institute of Physics, Vol. 7, pp. 729–734 (2003).
- [95] A. Ono, "Calculation of the Directional Emissivities of the Cavities by the Monte Carlo Method," *J. Opt. Soc. Am.* **70**, 547–554 (1980).
- [96] A. Ono, "Apparent Emissivities of Cylindrical Cavities with Partially Specular Conical Bottoms," in *Temperature: Its Measurement and Control in Science and Industry*, edited by J. F. Schooley, American Institute of Physics, Vol. 5, pp. 513–516 (1982).
- [97] A. Ono, R. M. Trusty, and D. P. DeWitt, "Experimental and Theoretical Study on the Quality of Reference Blackbodies Formed by Lateral Hole on a Metallic Tube," in *Temperature: Its Measurement and Control in Science and Industry*, edited by J. F. Schooley, American Institute of Physics, Vol. 5, pp. 541–550 (1982).
- [98] A. Ono, "Evaluation of the Effective Emissivity of Reference Sources for the Radiometric Emissivity Measurements," *Int. J. Thermophys.* **7**, 443–453 (1986).
- [99] A. V. Prokhorov, V. I. Sapritskii, and I. V. Klinger, "Statistical Modeling of the Radiation Characteristics of Specular–Diffuse Black-Body Models," *High Temp.* **28**, 99–105 (1990). Translated from: *Teplofizika Vysokikh Temperatur* **28**, 117–123 (1990).
- [100] G. A. Mikhailov, *Optimization of Weighted Monte Carlo Methods*, Springer, New York (1992).
- [101] A. Steinfeld, "Apparent Absorptance for Diffusely and Specularly Reflecting Spherical Cavities," *Int. J. Heat Mass Transfer* **34**, 1895–1896 (1991).

- [102] Z. Chu, J. Dai, and R. E. Bedford, "Monte Carlo Solution for the Directional Effective Emissivity of a Cylinder-Inner Cone," in *Temperature: Its Measurement and Control in Science and Industry*, edited by J. F. Schooley, American Institute of Physics, Vol. 6, pp. 907-912 (1992).
- [103] A. V. Prokhorov and L. M. Hanssen, "Effective Emissivity of a Cylindrical Cavity with an Inclined Bottom: I. Isothermal Cavity," *Metrologia* **41**, 421-431 (2004).
- [104] A. V. Prokhorov, S. N. Mekhontsev, and L. M. Hanssen, "Emissivity Modeling of Thermal Radiation Sources with Concentric Grooves," *High Temp.-High Pressures* **35/36**, 199-207 (2003/2004).
- [105] A. V. Prokhorov, L. M. Hanssen, and S. N. Mekhontsev, "Radiation Properties of IR Calibrators with V-Grooved Surfaces," *Proc. SPIE* **6205**, 620505 (2006).
- [106] *STEEP3 User's Guide*, Virial, Inc., New York (2000).
- [107] A. V. Prokhorov, "Monte Carlo Method in Optical Radiometry," *Metrologia* **35**, 465-471 (1998).
- [108] H. Zhang and J. Dai, "Evaluation on Effective Emissivity of a Surface with Homocentric V-Grooves by Monte-Carlo Method," in *Proceedings of Asia Simulation Conference/The Sixth International Conference on System Simulation and Scientific Computing*, Beijing, pp. 124-128 (2005).
- [109] H. Zhang and J. Dai, "A Novel Radiant Source for Infrared Calibration by Using a Grooved Surface," *Chin. Opt. Lett.* **4**, 306-308 (2006).
- [110] J. Ishii, M. Kobayashi, and F. Sakuma, "Effective Emissivities of Black-Body Cavities with Grooved Cylinders," *Metrologia* **35**, 175-180 (1998).
- [111] *OptiCAD User's Guide Ver. 4.0*, OptiCAD Co., New Mexico (1997).
- [112] T. J. Quinn and J. E. Martin, "A Black-Body Cavity for Total Radiation Thermometry," *Metrologia* **23**, 111-114 (1986/1987).
- [113] E. Usadi, "Reflecting Cavity Blackbodies for Radiometry," *Metrologia* **43**, S1-S5 (2006).
- [114] A. V. Prokhorov and J. E. Martin, "Monte Carlo Simulation of the Radiative Heat Transfer from a Blackbody to a Cryogenic Radiometer," *Proc. SPIE* **2815**, 160-168 (1996).
- [115] V. I. Sapritsky, S. N. Mekhontsev, A. I. Zhanov, and A. V. Prokhorov, "Numerical Modeling of Thermal and Radiative Characteristics of Low Temperature Blackbody with Wide Aperture," in *Proceedings of the International Conference of the Temperature and Thermal Measurements*, Beijing, pp. 129-133 (1997).
- [116] V. I. Sapritsky, S. N. Mekhontsev, A. V. Prokhorov, K. A. Sudarev, V. B. Khromchenko, and M. L. Samoilov, "Precision Large-Area Low- and Medium-Temperature Blackbody Sources," *Proc. SPIE* **3437**, 434-445 (1998).
- [117] S. N. Mekhontsev, V. I. Sapritsky, A. V. Prokhorov, V. B. Khromchenko, and M. L. Samoilov, "Modeling, Design, and Characterization of Medium-Background Blackbodies for Full-Aperture Calibration of Spaceborne Infrared Systems and Imagers," *Proc. SPIE* **3553**, 247-258 (1998).
- [118] M. R. Dury, T. Theocharous, N. Harrison, M. Hilton, and N. Fox, "The NPL Wide-Area MIR Calibration Source," *Proc. SPIE* **5405**, 532-540 (2004).
- [119] V. B. Khromchenko, S. N. Mekhontsev, and L. M. Hanssen, "Design and Evaluation of Large-Aperture Gallium Fixed-Point Blackbody," *Int. J. Thermophys.* **30**, 9-19 (2009).
- [120] V. I. Sapritsky and A. V. Prokhorov, "Calculation of the Effective Emissivities of Specular-Diffuse Cavities by the Monte Carlo Method," *Metrologia* **29**, 9-14 (1992).
- [121] V. I. Sapritsky and A. V. Prokhorov, "Spectral Effective Emissivities of Nonisothermal Cavities Calculated by the Monte Carlo Method," *Appl. Opt.* **34**, 5645-5652 (1995).

- [122] M. J. Ballico, "Modeling of the Effective Emissivity of a Graphite Tube Black Body," *Metrologia* **32**, 259–265 (1995/1996).
- [123] J. Hartmann, D. Taubert, and J. Fischer, "Characterization of the Double-Heatpipe Blackbody LABB for Use at Temperature Below 500°C," in *Proceedings of TEMPMEKO 1999, The Seventh International Symposium on Temperature and Thermal Measurements in Industry and Science*, edited by J. F. Dubbeldam and M. J. de Groot, NMI Van Swinden Laboratorium, Delft, pp. 511–516 (1999).
- [124] J. Hartmann, S. Schiller, R. Friedrich, and J. Fischer, "Non-isothermal Temperature Distribution and Resulting Emissivity Corrections for the High-Temperature Blackbody BB3200," in *Proceedings of TEMPMEKO 2001, The Eighth International Symposium on Temperature and Thermal Measurements in Industry and Science*, edited by B. Fellmuth, J. Seidel, and G. Scholz, VDI Verlag, Berlin, pp. 227–232 (2002).
- [125] J. Hartmann and D. Taubert, "Assessing Blackbody Emissivity by Monte Carlo Simulation," in *Proceedings of Seventh International Conference on Infrared Sensors and Systems (IRS<sup>2</sup> 2002)*, edited by G. Gerlach, Wunstorf, AMA Service-GmbH, Erfurt, Germany, pp. 133–138 (2002).
- [126] A. V. Murthy, A. V. Prokhorov, and D. P. DeWitt, "High Heat-Flux Sensor Calibration: A Monte Carlo Modeling," *J. Thermophys. Heat Transfer* **18**, 333–341 (2004).
- [127] J. Ishii, T. Fukuzaki, T. Kojima, and A. Ono, "Calibration of Infrared Ear Thermometers," in *Proceedings of TEMPMEKO 2001, The Eighth International Symposium on Temperature and Thermal Measurements in Industry and Science*, edited by B. Fellmuth, J. Seidel, and G. Scholz, VDI Verlag, Berlin, pp. 729–734 (2002).
- [128] J. Zaworski, J. R. Welty, B. J. Palmer, and M. K. Drost, "Comparison of Experiment with Monte Carlo Simulations on a Reflective Gap Using a Detailed Surface Properties Model," *J. Heat Transfer* **118**, 388–393 (1996).
- [129] K. E. Torrance and E. M. Sparrow, "Theory for Off-Specular Reflection from Roughened Surfaces," *J. Opt. Soc. Am.* **57**, 1105–1114 (1967).
- [130] Y. H. Zhou, Z. M. Zhang, D. P. DeWitt, and B. K. Tsai, "Effects of Radiative Properties of Surfaces on Radiometric Temperature Measurement," in *Proceedings of Ninth International Conference on Advanced Thermal Processing of Semiconductors (RTP 2001)*, edited by D. P. DeWitt, J. Gelpey, B. Lojek, and Z. Nenyeyi, IEEE, Anchorage (AK), pp. 179–188 (2001).
- [131] G. J. Ward, "Measuring and Modeling Anisotropic Reflection," *Comput. Graphics* **26**, 265–272 (1992).
- [132] A. V. Prokhorov, S. N. Mekhontsev, and L. M. Hanssen, "Radiative Properties of Blackbody Calibration Sources: Recent Advances in Computer Modeling," *Int. J. Thermophys.* **28**, 2128–2144 (2007).
- [133] L. M. Hanssen and A. V. Prokhorov, "A Procedural Model of Reflection from Random Rough Surfaces," *Proc. SPIE* **7065**, 70650W (2008).
- [134] H. C. McEvoy, G. Machin, R. Friedrich, J. Hartmann, and J. Hollandt, "Comparison of the New NPL Primary Standard Ag Fixed-Point Blackbody Source with the Primary Standard Ag Fixed-Point of PTB," in *Temperature: Its Measurement and Control in Science and Industry*, edited by D. C. Ripple, Vol. 7, pp. 909–914 (2003).